Millimeter-Wave Spectra of Metal Sulfides and Related Astronomical Searches

金属硫化物のミリ波スペクトル及びそれらの星間での探査

A Thesis for the Degree of Doctor of Science
Submitted to Department of Astrophysics,
Faculty of Science, Nagoya University

by Shuro Takano in December, 1990

名古屋大学理学研究科宇宙理学　高野秀路

(1)

Millimeter-Wave Spectra of Metal Sulfides and Related Astronomical Searches

金属硫化物のミリ波スペクトル及びそれらの星間での探査

A Thesis for the Degree of Doctor of Science
Submitted to Department of Astrophysics,
Faculty of Science, Nagoya University

by Shuro Takano in December 1990

ACKOWLEDGMENT

The author withes to express his sincere gratitude to Professor Shuji Saito for his helpful guidance and valuable suggestions throughout this work. The author is also grateful to Dr. Satoshi Yamamoto for his helpful suggestions.

The radioastronomical observations in this work were carried out at Nobeyama Radio Observatory under close collaboration with Drs. Norio Kaifu, Kentarou Kawaguchi, Masatoshi Ohishi, and Shin-ichi Ishikawa. The author thanks them for their helpful comments and supports in the observations.

The thermal equilibrium calculations for carbon-rich atmosphere were carried out by Dr. Takashi Tsuji. The author is grateful to him for his helpful comments on the calculations.

The author thanks the staff members of the Instrumental Development Center of Faculty of Science, Nagoya University for their construction of the high-temperature cell used in this study.

The author thanks Dr. Mitsutoshi Tamimoto for lending him a klystron (OKI KA1330) used in this study.

The author is also grateful to all the member of our laboratory, Hitomi Mikami, Mitsuka Kanada, François Xavier Brown, Mitsuaki Izuha, Mizuho Tonooka, and Shin-ichi Hayakashi, for their encouragement in this work.

CONTENTS

Chapter 1. Introduction

ABSTRACT

Molecules observed in circumstellar envelopes of late-type stars were briefly reviewed. Many molecules have been found in the carbon-rich circumstellar envelope of a red giant star IRC+10216 in millimeter-wave region. In this envelope, several molecules containing refractory elements have been detected, but molecules containing Mg, Ca, and Fe have not been found. According to a thermal equilibrium model for stellar atmospheres, the envelope might be relatively abundant in metal sulfides, especially Mg, Ca, and Fe containing species.

1-1. Molecules in Space

Knowledge of molecules in interstellar space and circumstellar envelopes is important to understand chemistry in extreme physical conditions of density and temperature, and in long time scale which cannot be realized in the laboratory. The molecules are also important as a probe of physical conditions in interstellar space and circumstellar envelopes.

The first molecules found in interstellar space were CH, CH^+, and CN. These molecules were discovered by optical absorption spectroscopy toward the background stars (Swings and Rosenfeld 1937; Mckellar 1940; Douglas and Herzberg 1941). Until the detections of these molecules, the interstellar matter was considered to exist in the atomic form under the influence of interstellar UV radiation. The detection of molecules indicates that the material in interstellar space is not only in the atomic form, and that the molecules are formed in interstellar space. This discovery changed the recognition of astronomers about the interstellar matter.

Then, many interstellar molecules have been discovered with the radioastronomical techniques from 1960's: OH (Weinreb et al. 1963), NH_3 (Cheung et al. 1968), H_2O (Cheung et al. 1969), and so on. In the early stage of the discovery by radioastronomy, various kinds of stable and known molecules ever studied in the laboratory were found, while most of the molecules recently found were radicals. In total, about 80 molecules have been found in space. These molecules have been detected in relatively dense region ($\geq 10^2$ atoms per cm^3) in space: (1) the Sagittarius region (our galactic center), which is a complex of giant molecular clouds, ionized (HII) regions, and stars, (2) molecular clouds including cold dark clouds, low mass star forming regions, and massive star forming regions, and (3) late type stars with circumstellar envelopes.

The discovery of many interstellar molecules has opened a way to a new field of chemistry in space. It is a great surprise that many molecules are produced in low-density ($10^2 \sim 10^5$ molecules per cm^3) and low-temperature ($\geq$ 10 K) interstellar space.

General chemical reactions known in the laboratory, such as neutral-neutral reactions, thermal reactions, and endothermic reactions are completely ineffective for production of molecules in the interstellar physical conditions given above. In this situation, the ion-molecule reaction was proposed to explain production of various molecules in low density and low temperature region (Solomon and Klemperer 1972; Watson 1973 and 1974; Herbst and Klemperer 1973), and now, the ion-molecule reaction has been considered to be one of the main mechanisms for production and destruction of molecules in cold space. However, there are several observational results which cannot be explained only by the ion-molecule reaction. Other processes such as grain surface reactions, and high-temperature reactions introduced by shock wave and by stellar radiation have been suggested for such cases.

The discovery of interstellar molecules also gave a useful probe of the physical condition of interstellar matter. Radiotelescopes can observe the rotational transitions of molecules in centimeter-wave and millimeter-wave regions which correspond to several degrees of Kelvin in energy. Therefore, molecular spectral lines are useful and valuable probes to observe low temperature phenomena ($\geq$ 10 K) in space. For example, the spectral lines of CO is widely used to study the distribution (structure) and the physical condition of interstellar matter, because the abundance of CO is considered to be proportional to the hydrogen abundance.

1-2. Circumstellar Envelopes

In the last stage of stellar evolution, stars with about one solar mass become red giant stars and eject the surface of themselves into circumstellar space. This activity is called "mass loss" and consequently the gas and dust form shells around red giant stars. These shells are called "circumstellar envelope". The circumstellar envelope evolves to a planetary nebula as the central star evolves to white dwarf. In circumstellar envelopes, molecules are produced and the rotational transitions of various molecules have been detected by radiotelescopes. The recent developement of radiotelescopes with large

diameter has made it possible to study the circumstellar envelopes in detail.

The observation of molecules in circumstellar envelopes has two aspects. (1) The understanding of chemical processes in circumstellar envelopes. (2) The understanding of stellar evolution based on the physical conditions deduced from molecular observational results. The present thesis deals with the former aspect.

1-3. Molecules Found in Circumstellar Envelopes

The most extensively surveyed molecule in circumstellar envelopes is CO (for example, Knapp and Morris 1985; Zuckerman, Dyck, and Claussen 1986), and the analysis of the CO spectral lines yields the stellar central velocities, the terminal outflow velocities of the envelope, and the mass loss rates. The second molecule which has been surveyed in circumstellar envelopes is HCN (Zuckerman, and Dyck, 1986; Lucas, Guilloteau, Omont 1988; Izumiura 1990). Generally, the emission from HCN is detected in carbon-rich circumstellar envelopes, while only the weak emission is observed in oxygen-rich circumstellar envelopes (Deguchi and Goldsmith 1985). Therefore, the emission from HCN is useful to a distinction of the envelopes: oxygen-rich or carbon-rich.

The abundant molecules next to HCN are CN, CS, HC_3N, and so on. In the carbon-rich circumstellar envelope of a red giant star IRC+10216, the abundances of CN, CS, and HC_3N relative to CO are 2.8×10^{-3}, 1.8×10^{-5}, and 1.8×10^{-5}, respectively (McCabe, Smith, and Clegg 1979). Because of their low abundances, the observations of molecules other than CO and HCN have been limited to several circumstellar envelopes. (In the case of maser emissions, OH, H_2O, and SiO have been detected in many envelopes (Olofsson 1988).) The list of observed molecules in circumstellar envelopes is shown in Table 1. There are a few circumstellar envelopes where several molecules have been detected. Such envelopes are IRC+10216 (McCabe, Smith, and Clegg 1979), CRL2688, CRL618 (Bujarrabal et al. 1988), and CIT6 (Henkel et al. 1985). These envelopes contain the carbon-rich material. On the other hand, only one oxygen-rich envelope is known to have

rich molecular lines. That is OH231.8+4.2 (Morris et al. 1987). In particular, several sulfur bearing molecules such as SO, SO_2, CS, and OCS were found in this envelope.

1-4. Introduction to the Carbon-Rich Circumstellar Envelope of a Red Giant Star IRC+10216 and the Chemistry

IRC+10216 is the brightest infrared object at 10 μm except the solar system, and show the richest molecular spectral lines. The molecules found in IRC+10216 have two characteristics. (1) The existence of series of carbon-chain molecules, such as C_n (n=3 Hinkle, Keady, and Bernath 1988, n=5 Bernath, Hinkle, and Keady 1989), C_nH (n=2 to 6 Saito et al. 1987 and references in their paper), C_nN (n=3 Guélin and Thaddeus 1977), C_nS (n=2 and 3 Cernicharo et al. 1987), C_nH_2 (n=3 tentative detection, Cernicharo et al. 1990a; n=4 Cernicharo et al. 1990b), and C_nSi (n=4 Ohishi et al. 1989), and $HC_{2n+1}N$ (n=1 Morris 1975, n=2 and 3 Winnewisser and Walmsley 1978, n=4 Matthews, Friberg, and Irvine 1985, n=5 Bell et al. 1982). Both C_3 and C_5 molecules were detected with infrared absorption spectrometry. Most of these carbon-chain molecules are also abundant in a cold dark cloud TMC-1. (2) The existence of molecules containing refractory elements, such as SiO and SiS (Morris 1975), SiC_2 (Thaddeus, Cummins, and Linke 1984), SiC (Cernicharo et al. 1989), SiC_4 (Ohishi et al. 1989), SiH_4 (Goldhaber and Betz 1984), NaCl, KCl, AlCl, and AlF (Cernicharo and Guélin 1987), and CP (Guélin et al. 1990). No molecules containing refractory elements have been detected in cold dark clouds.

The spatial distributions in the envelope of IRC+10216 have been obtained for some of these molecules by interferometric observations. Based on these results, the relation between the distribution and the reaction has been discussed. The distributions of HCN (Bieging, Chapman, and Welch 1984), HC_3N, HNC, and C_2H (Bieging and N-Q-Rieu 1988), SiS (Bieging and N-Q-Rieu 1989), and CS (Kasuga, Mikami, and Takano 1991) have been studied. The results show that HCN, SiS, and CS concentrate in the

central region. This fact means that these molecules mainly exist in the inner envelope. On the other hand, HC_3N, HNC, and C_2H are mainly present in the outer envelope forming a spherical shell and their abundances at the central region are low. The peak positions of HC_3N, HNC, and C_2H are located at the radial distances of $4.5x10^{16}$, $4x10^{16}$, and $6x10^{16}$ cm, respectively, from the central star. Most of HCN, SiS, and CS were produced in the inner envelope where the density and the temperature are relatively high, and consequently their productions are considered to be determined by the thermal equilibrium condition modified by reactions between neutral species. On the other hand, most of HC_3N, HNC, and C_2H were produced in the outer envelope where the density and the temperature are relatively low. The reactions responsible for them are considered to be ion-molecule reaction and photochemical reaction. The distribution of HC_3N, HNC, and C_2H are consistent with those predicted by chemical models for the outer envelope (Glassgold et al. 1987; Nejad and Millar 1987). The models predict that the molecules are distributed in the region between 10^{16} and 10^{17} cm from the central star. Figure 1 shows schematically how the reactions in the envelope change by the distance from the central stars. The rich molecular lines in IRC+10216 are considered to be due to the active molecular production, that is the high rate mass loss, and the short distance (200pc) from the earth. Therefore, IRC+10216 is the important astronomical object in understanding the chemistry of not only the envelope of IRC+10216 itself, but other carbon-rich circumstellar envelopes.

1-5. Problems in the Chemistry in IRC+10216

So far, Mg, Ca, and Fe containing molecules have not been detected in the envelope of IRC+10216. In Table 2, elements are listed in the order of their cosmic abundances. The relatively high cosmic abundances of these atoms suggest that Mg, Ca, and Fe containing molecules are expected to be abundant in circumstellar envelopes. However, MgO (Turner and Steimle 1985; Millar et al. 1987), MgCl (Demuynck 1990), CaO (Hocking

et al. 1979), CaCl (Cernicharo and Guélin 1987), CaOH (Saito et al. 1990), and FeO (Merer, Walmsley, and Churchwell 1982; Cernicharo and Guélin 1987) have been searched for without success. The study of these refractory molecules will contribute to an understanding of the chemistry in the high-temperature inner envelope (Figure 1). The chemistry is closely related to the grain formation. The existence of MgS grain in the envelope of IRC+10216 is suggested from a far-infrared spectrophotometry (Goebel and Moseley 1985).

Tsuji (1973) calculated molecular abundances in stellar atmospheres assuming thermal equilibrium which is atteined at the beginning stage of the mass loss process (Figure 1). According to his calculation, "metal sulfides" are predicted to be relatively abundant. In particular, the abundances of metal sulfides, MgS, CaS, AlS, and FeS, are larger than those of the corresponding metal oxides in cool stellar envelopes such as IRC+10216 (1600 K, Lafont, Lucas, and Omont 1982) as shown in Figures 2 ~ 5. Tsuji's calculation (1973) was mainly carried out under oxygen-rich conditions while IRC+10216 has a carbon-rich envelope. This suggests a possibility of high abundances of the metal sulfides in the envelope of IRC+10216, when compared with those of the corresponding metal oxides. The metal sulfides are good candidates for carriers of metals such as Mg, Ca, and Fe. However, searches for these metal sulfides have not been carried out, because the spectroscopic data with sufficient accuracy for their identification in space were not reported.

In this situation, the author began to study the spectra of these metal sulfides by millimeter-wave spectroscopy, aiming to understand the chemistry and physics of molecules in the circumstellar envelope.

1-6. Outline of This Thesis

In the next Chapter, spectroscopy of metal containing molecules is reviewed, and the construction of a high-temperature cell used in this study is explained. In Chapter 3, millimeter-wave spectroscopy of four metal sulfides, MgS, CaS, AlS, and FeS, is described.

MgS, CaS, and AlS were produced by reactions between the corresponding metal vapor and a sulfur containing molecule in the high-temperature cell, while FeS was more effectively produced by the hollow cathode discharge in the mixture of Ar and H_2S in a free space cell. In Chapter 4, the searches for the metal sulfides toward the carbon-rich envelope IRC+10216 and other sources were described.

REFERENCES

Bell, M.B., Feldman, P.A., Kwok, S., and Matthews, H.E. 1982, Nature, **295**, 389.

Bernath, P.F., Hinkle, K.H., and Keady, J.J. 1989, Science, **244**, 562.

Bieging, J.H., Chapman, B., and Welch, W.J. 1984, Astrophys. J., **285**, 656.

Bieging, J.H., and N-Q-Rieu 1988, Astrophys. J., **329**, L107.

Bieging, J.H., and N-Q-Rieu 1989, Astrophys. J., **343**, L25.

Bujarrabal, V., Gomez-Gonzalez, J., Bachiller, R., and Martín-Pintado, J. 1988, Astron. Astrophys., **204**, 242.

Cernicharo, J., Gottlieb, C.A., Guélin, M., Killian, T.C., Paubert, G., Thaddeus, P., and Vrtilek, J.M. 1990a, Astrophys. J., submitted.

Cernicharo, J., Gottlieb, C.A., Guélin, M., Killian, T.C., Thaddeus, P., and Vrtilek, J.M. 1990b, Astrophys. J., submitted.

Cernicharo, J., Gottlieb, C.A., Guélin, M., Thaddeus, P., and Vrtilek, J.M. 1989, Astrophys. J., **341**, L25.

Cernicharo, J., and Guélin, M. 1987, Astron. Astrophys., **183**, L10.

Cernicharo, J., and Guélin, M., Hein, H., and Kahane, C. 1987, Astron. Astrophys., **181**, L9.

Cheung, A.C., Rank, D.M., Townes, C.H., Thornton, D.D., and Welch, W.J., 1968, Phys. Rev. Lett., **21**, 1701.

Cheung, A.C., Rank, D.M., Townes, C.H., Thornton, D.D., and Welch, W.J., 1969, Nature, **221**, 626.

Deguchi, S., and Goldsmith, P.F. 1985, Nature, **317**, 336.

Demuynck, C. 1990, 20th International symposium on free radicals, Susono, Japan.

Douglas, A.E., and Herzberg, G. 1941, Astrophys.J., **94**, 381.

Glassgold, A.E., Mamon, G.A., Omont, A., and Lucas, R. 1987 Astron. Astrophys., **180**, 183.

Goebel, J.H., and Moseley, S.H. 1985, Astrophys. J., **290**, L35.

Goldhaber, D.M., and Betz, A.L. 1984, Astrophys. J., **279**, L55.

Guélin, M., Cernicharo, J., Navarro, S., Woodward, D.R., Gottlieb, C.A., and Thaddeus, P. 1987, Astron. Astrophys., **182**, L37.

Guélin, M., Cernicharo, J., Paubert, G., and Turner, B.E. 1990, Astron. Astrophys., **230**, L9.

Guélin, M., and Thaddeus, P. 1977, Astrophys. J., **212**, L81.

Henkel, C., Matthews, H.E., Morris, M., Terebey, S., and Fich, M. 1985, Astron. Astrophys., **147**, 143.

Herbst, E., and Klemperer, W. 1973, Astrophys. J., **185**, 505.

Hinkle, K.H., Keady, J.J., and Bernath, P.F. 1988, Science, **241**, 1319.

Hocking, W.H., Winnewisser, G., Churchwell, E., and Percival, J. 1979, Astron. Astrophys., **75**, 268.

Izumiura, H. 1990, Ph.D. thesis (University of Tokyo).

Kasuga, T., Mikami,H., and Takano, S. 1991 to be published.

Knapp, G.R., and Morris, M. 1985, Astrophys. J., **292**, 640.

Lafont, S., Lucas, R., and Omont, A. 1982, Astron. Astrophys., **106**, 201.

Lucas, R., Guilloteau, S., and Omont, A. 1988, Astron. Astrophys., **194**, 230.

Matthews, H.E., Friberg, P., and Irvine, W.M. 1985, Astrophys. J., **290**, 609.

McCabe, E.M., Smith, R.C., and Clegg, R.E.S. 1979, Nature, **281**, 263.

McKellar, A. 1940, Publ. Astron. Soc. Pacific, **52**, 187.

Merer, A.J., Walmsley, C.M., and Churchwell, E. 1982, Astrophys. J., **256**, 151.

Morris, M. 1975, Astrophys. J., **197**, 603.

Morris, M., Guilloteau, S., Lucas, R., and Omont, A. 1987, Astrophys. J., **321**, 888.

Millar, T.J., and Elldér, J., Hjalmarson, Å, and Olofsson H. 1987, Astron. Astrophys., **182**, 143.

Nejad, L.A.M., and Millar, T.J. 1987, Astron. Astrophys., **183**, 279.

Ohishi, M., Kaifu, N., Kawaguchi, K., Murakami, A., Saito, S., Yamamoto, S., Ishikawa, S.,

Fujita, Y., Shiratori, Y., and Irvine, W.M. 1989, Astrophys. J., **345**, L83.

Olofsson, H. 1988, Space Science Reviews, **47**, 145.

Saito, S., Takano, S., and others 1990, to be published.

Saito, S., Kawaguchi, K., Suzuki, H., Ohishi, M., Kaifu, N., and Ishikawa, S. 1987, Publ. Astron. Soc. Japan, **39**, 193.

Solomon, P.M., and Klemperer, W. 1972, Astrophys. J., **178**, 389.

Swings, P., and Rosenfeld, L. 1937, Astrophys. J., **86**, 483.

Thaddeus, P., Cummins, S., and Linke, R.A. 1984, Astrophys. J., **283**, L45.

Tsuji, T. 1973, Astron. Astrophys., **23**, 411.

Turner, B.E., and Steimle, T.C. 1985, Astrophys. J., **299**, 956.

Watson, W.D. 1973, Astrophys. J., **183**, L17.

Watson, W.D. 1974, Astrophys. J., **188**, 35.

Weinreb, S., Barret, A.H., Meeks, M.L., and Henry, J.C. 1963, Nature, **200**, 829.

Winnewisser, G., and Walmsley, C.M. 1978, Astron. Astrophys., **70**, L37.

Zuckerman, B., and Dyck, H.M. 1986, Astrophys. J., **311**, 345.

Zuckerman, B., Dyck, H.M., and Claussen, M.J. 1986, Astrophys. J., **304**, 401.

TABLE 1

Molecules detected at radio wavelength in circumstellar envelopes[a]

Molecule	Number of sources	
	C-rich	O-rich
CO	≈125	≈100
CN	3	
CS	6	1
CP	1	
SiC	2	
SiO(thermal)	3	≈30
SiS	4	
SiC_2	4	
SiC_4	1	
SO		7
SO_2		7
H_2S		1
OCS		1
HCO^+	3	2
HCN	≈50	9
CH_3CN	1	
HNC	5	1
NH_3	2	1
HC_3N	6	
HC_5N	3	
HC_7N	2	
HC_9N	1	
$HC_{11}N$	1	
C_2H	3	
C_3H	2	
C_3H_2 (cyclic)	3	
C_3H_2 (linear)(?)	1	
C_4H_2 (linear)	1	
C_4H	3	
C_5H	1	
C_6H	1	
C_3N	4	
C_2S	1	
C_3S	1	
$HSiC_2$ (HSC_2)(?)	1	
NaCl	1	
AlCl	1	
KCl	1	
AlF	1	
OH(maser)		> 1000
H_2O(maser)	2	≈200
SiO(maser)		≈140

[a] Based on Olofsson (1988).

TABLE 2
The cosmic abundances of the elements.

Element	Abundance [a]	Fractional Abundances[b]	Example of Known Molecules in Space
H	10.50	—	HCN
He	9.34	–0.86	—
O	7.33	–2.87	CO
C	7.07	–3.13	CO, CS
N	6.57	–3.63	CN, HCN
Ne	6.53	–3.67	—
Mg	6.02	–4.18	—
Si	6.00	–4.20	SiO, SiS
Fe	5.94	–4.26	—
S	5.69	–4.51	SiS, CS
Al	4.92	–5.28	AlCl, AlF
Ca	4.85	–5.35	—
Na	4.77	–5.43	NaCl
Ni	4.67	–5.53	—
Cr	4.09	–6.11	—
Mn	3.96	–6.51	—
P	3.93	–6.27	CP
Cl	3.76	–6.44	NaCl, KCl
K	3.58	–6.62	KCl
F	3.39	–6.81	AlF
Ti	3.38	–6.82	—
Co	3.34	–6.86	—

[a]The abundance was normalized by that of silicone, $\log_{10}\mathrm{Si} = 6$.
[b]Relative to H_2.

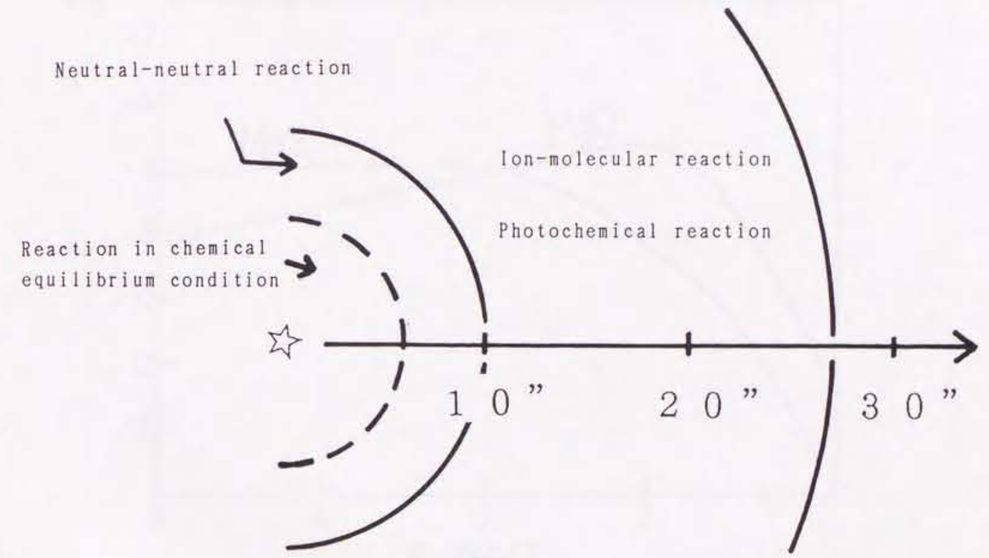

Figure 1: The schematic drawing of the type of reactions by the distance from the central star. The scale indicates the distance by arcsecond. The positions of the shell for ion-molecule reaction and photochemical reaction are shown on the basis of the HC_3N distribution in the envelope of IRC+10216 (Bieging and N-Q-Rieu 1988).

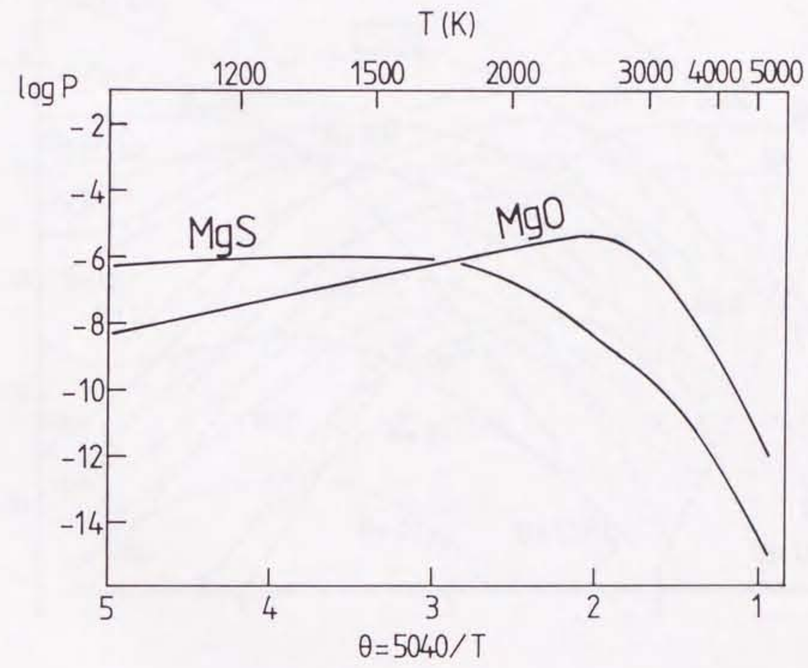

Figure 2: The abundance of MgS calculated assuming thermal equilibrium by Tsuji (1973). The ordinate is the partial pressure of the molecule.

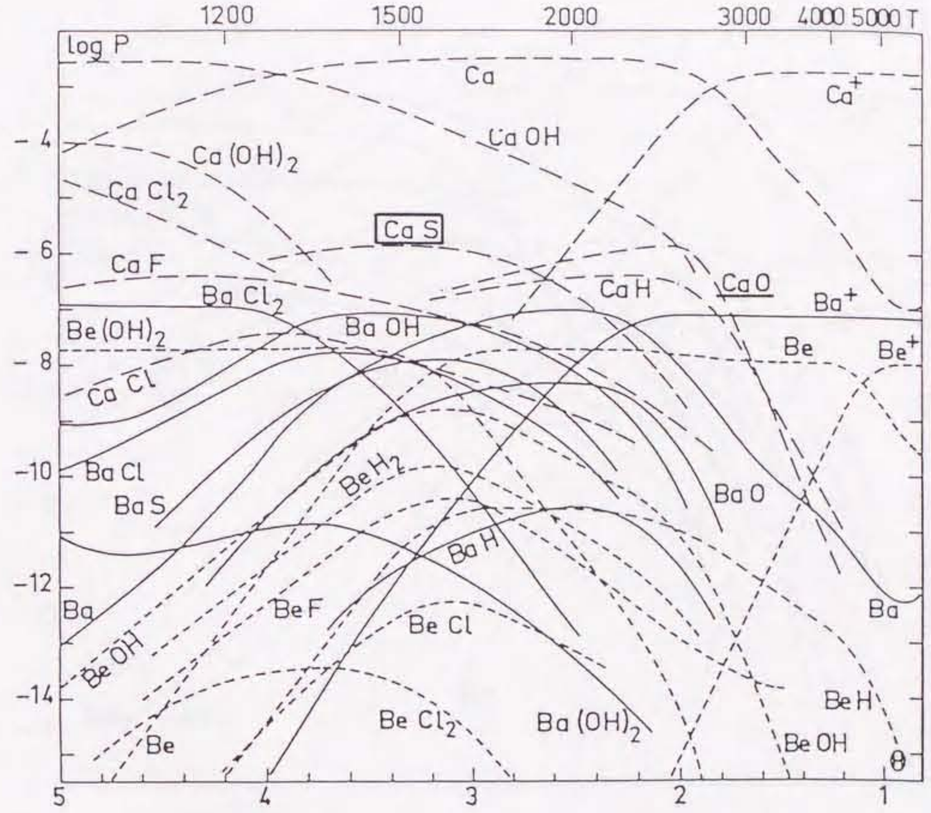

Figure 3: The abundance of CaS calculated assuming thermal equilibrium by Tsuji (1973). The ordinate is the partial pressure of the molecule.

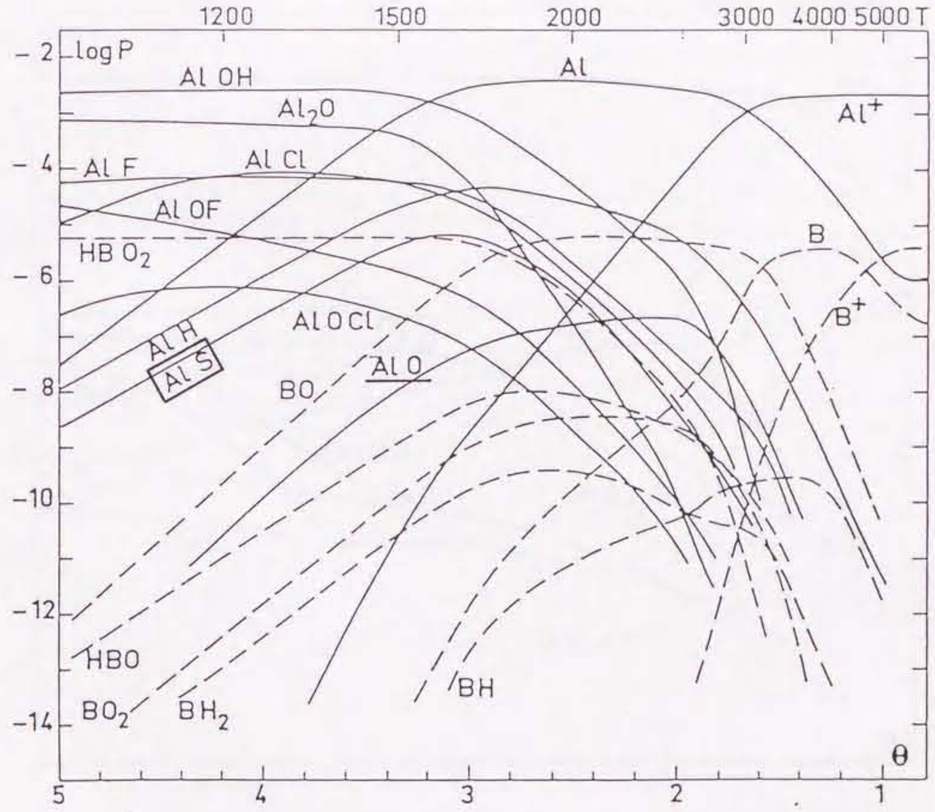

Figure 4: The abundance of AlS calculated assuming thermal equilibrium by Tsuji (1973). The ordinate is the partial pressure of the molecule.

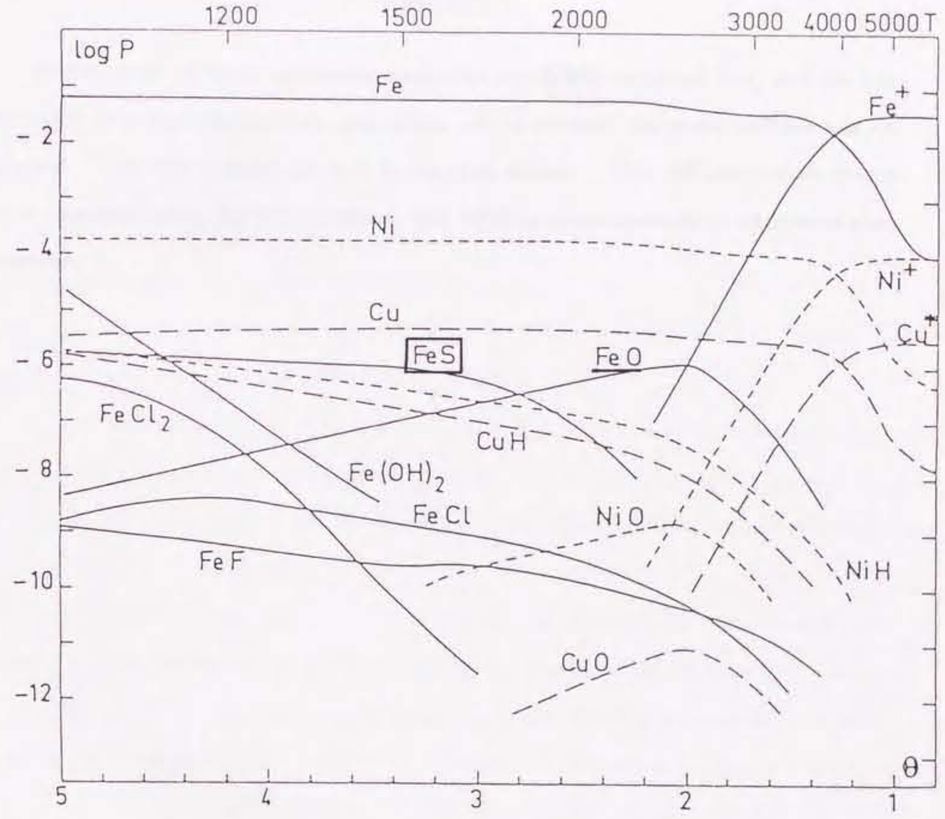

Figure 5: The abundance of FeS calculated assuming thermal equilibrium by Tsuji (1973). The ordinate is the partial pressure of the molecule.

Chapter 2. High-Temperature Microwave Spectroscopy and the High-Temperature Cell

ABSTRACT

Spectroscopy of metal containing molecules was briefly reviewed first, and the construction of a high-temperature absorption cell to produce the metal sulfides was explained. The cell contains an oven to vaporize metals. The millimeter-wave spectra were measured using this cell combined with 100 kHz source-modulated microwave spectrometer.

2-1. Spectroscopy of Metal Containing Molecules

Several production methods have been presented for spectroscopy of low vapor pressure molecules including metal containing molecules, in optical, infrared, and microwave (centimeter-wave and millimeter-wave) regions.

In optical spectroscopy, the richest spectral data have been obtained for metal containing molecules (Huber and Herzberg 1979), mainly because of its high sensitivity. Two methods have been often employed to produce molecules. (1) The discharge of gases by electrodes made of an appropriate metal. The metal is supplied from the electrode to the gas phase. For example, IrO was produced by this method (Jansson and Scullman 1972). (2) The heating of materials in an oven to increase their vapor pressure. For example, the electronic spectrum of such as CaS (Blues and Barrow 1969) and AlS (Kronekvist and Lagerqvist 1969) were obtained by this method.

In infrared spectroscopy, the metal containing molecules are much less studied than those studied by optical spectroscopy. The method often used is to vaporize samples in a heat pipe cell. This method was extensively applied to the production of metal hydrides such as AgH (Birk and Jones 1989).

In the centimeter- and millimeter-wave regions, the development of high-temperature cells has made possible the study of the rotational spectra of molecules which have too low a vapor pressure at room temperature. However, the data of the metal containing molecules are limited. There are several advantages in centimeter-wave and millimeter-wave spectroscopy. (1) The accuracy is relatively high in the frequency measurements. This means that the precise molecular constants are obtained. (2) Because of the high resolution, information on the hyperfine structure can be easily obtained. (3) Generally, it is easy to obtain information on the ground electronic state of the molecule. (4) The transition frequency determined is directly applicable to observations and identifications of interstellar molecules by radiotelescopes.

The study of metal containing molecules in the centimeter-wave and millimeter-wave

regions is reviewed in more detail. The first work of centimeter-wave spectroscopy by using a high-temperature absorption cell was carried out by Townes' group. They used a heated waveguide cell. This method was applied to observations of several alkali halides such as NaCl and KCl (Honig et al. 1954). Later, this type of the high-temperature cell was also employed by Lide, Cahill, and Gold (1964), Fitzky (1958), Hoeft (1961), and Törring (1964). Later Winnewisser (1981) constructed a free space cell with an oven. This cell was suitable for millimeter-wave spectroscopy. Millimeter-wave radiation can be easily collimated into the cell by horns and Teflon lenses. Furthermore, the sensitivity of the spectrometer is improved in the millimeter-wave region by the increase of the line strength, because the line strength is proportional to the square or cube of the transition frequency. The rotational spectra of $^1\Sigma$ molecules containing refractory elements were extensively measured in 1950's to 1970's with these high-temperature cells. Most of them were metal halides and metal oxides.

In 1980's, the measurements of the rotational spectra of metal containing radicals started by using high-temperature cells in millimeter-wave region. In 1980, Ryzlewicz and Törring measured the rotational spectrum of a $^2\Sigma$ radical BaF. They used both of a waveguide cell and a free space cell. Then, the measurements of several $^2\Sigma$ alkali earth halides followed; BaCl (Ryzlewicz et al. 1982), CaCl, CaBr (Möller et al. 1982), SrF, SrCl (Schütze-Pahlmann et al. 1982), and MgCl (Bogey, Demuynck, and Destombes 1989). At Institute for Molecular Science, the spectrum of FeO ($X^5\Delta_i$) (Endo, Saito, and Hirota 1984) was measured by discharging a mixture of ferrocene and oxygen in a free space cell. Furthermore, Yamada et al. extensively studied the rotational spectra of alkali oxides, LiO (Yamada, Fujitake, and Hirota 1989a), NaO (Yamada, Fujitake, and Hirota 1989b), KO, RbO, and CsO (Yamada, Fujitake, and Hirota 1990a) by using a heat pipe cell. The ground electronic states of LiO, NaO, and KO were $^2\Pi$ while that of RbO and CsO $^2\Sigma$. More recently they measured the rotational spectrum of AlO ($X^2\Sigma$) by using a combination of a free space cell and an oven to vaporize metal (Yamada et al.

1990b). The rotational spectrum of AlO was also measured by Törring and Herrmann (1989) by using a high-temperature cell.

As reviewed above, the rotational spectra of the metal containing molecules with low melting points (< 1000 ℃) have been studied so far with high-temperature cells. Few studies have been made on metal sulfides. Some of them are important to astrochemistry as discussed in the former Chapter, and millimeter-wave spectroscopy of metal sulfides may give useful information on the identification of these molecules in space. The author constructed a high-temperature cell to measure the rotational spectra of metal sulfides.

2-2. Construction of a High-Temperature Cell for Metal Sulfides

The author constructed a reaction chamber to produce metal sulfides, which are potential carriers of Mg, Ca, and Fe in IRC+10216, by the reaction between vaporized metals and reactant gases. So as to vaporize metals such as Mg, Ca, Al and Fe, the temperature of the oven must be above 1800 K. For this purpose, the author designed a cell equipped with a high-temperature crucible made of non-melting materials at 1500 ~ 2000 K such as carbon and alumina. The schematic cross sections of the chamber, which are made of a cylindrical stainless steel, are shown in Figure 1(a) and 1(b). The height is 30 cm and the diameter is 40 cm. The chamber has eight ports separated from one another by 45 °. A pair of facing ports, which are sealed with Teflon lenses, are used as input and output windows for microwave transmission. Other ports are used for introduction of reactant and carrier gases, for pumping of gases by a turbomolecular pump (270 liter s^{-1} for N_2), for supplying electricity (6 V 500 A at maximum) for the heater, for vacuum gauges, and for a glass window. The chamber is equipped with an oven, which is shown in Figure 2, bearing a crucible to produce metal vapor. The oven is placed just below the path of microwave transmission (Figure 1(a)). The electricity is supplied to the oven through copper tubes of 6 mm in diameter (Figure 1(b)). Water is passed through the tube to cool the electrodes of the oven. The stainless steel chamber

is also cooled by passing water through the stainless steel tube which is attached to the chamber. When paramagnetic molecules are produced in the cell, the Helmholtz coil is placed at the outside of the cell to cancel the magnetic field of the earth.

As shown in Figure 2, the crucible in the oven is surrounded by a tantalum foil (0.05 mm thick) which serves as a resistance heater. The maximum temperature achieved by this oven was about 1600 K, measured by an optical pyrometer. For the construction of the chamber, the author refered to the oven for optical spectroscopy (West et al. 1975). When the author tried to measure the millimeter-wave spectrum of FeS, another oven was used. The fundamental structure of the oven is the same, but the material of the oven is molybdenum instead of stainless steel. The maximum temperature achieved by this oven was about 2200 K.

The crucibles used are made of carbon, stainless steel, or alumina. The choice of the crucible is very important to vaporize metals. The crucible and metals must not react rapidly, and the melting point of the crucible must be higher than those of samples.

This newly constructed high-temperature cell was combined with the 100 kHz source-modulated microwave spectrometer (Yamamoto and Saito 1988) to measure the rotational spectra of the metal sulfides; MgS, CaS, AlS, and FeS.

REFERENCES

Birk, H., and Jones, H. 1989, Chem.Phys.Lett., **161**, 27.

Blues, R.C., and Barrow, R.F. 1969, Trans. Faraday Soc., **65**, 646.

Bogey, M., Demuynk, C., and Destombes, J.L. 1989, Chem.Phys.Lett., **155**, 265.

Endo, Y., Saito, S., and Hirota, E. 1984, Astrophys. J., **278**, L131.

Fitzky, H.G. 1958, Z. Physik, **151**, 351.

Hoeft, J. 1961, Z. Physik, **163**, 262.

Honig, A., Mandel, M., Stitch, M.L., and Townes, C.H. 1954, Phys. Rev., **96**, 629.

Huber, K.P., and Herzberg, G. 1979, Constants of Diatomic Molecules
(Van Nostrand, New York).

Jansson, K., and Scullman, R. 1972, J. Mol. Spectrosc., **43**, 208.

Kronekvist, M., and Lagerqvist, A. 1969, Arkiv för Fysik, **39**, 133.

Lide, Jr., D.R., Cahill, P., and Gold, L.P. 1964, J. Chem. Phys., **40**, 156.

Möller, K., Schütze-Pahlmann, H.U., Hoeft, J., and Törring, T. 1982,
Chem. Phys., **68**, 399.

Ryzlewicz, Ch., Schütze-Pahlmann, H.U., Hoeft, J., and Törring, T. 1982,
Chem. Phys., **71**, 389.

Ryzlewicz, Ch., and Törring, T. 1980, Chem. Phys., **51**, 329.

Schütze-Pahlmann, H.U., Ryzlewicz, Ch., Hoeft, J., and Törring, T. 1982,
Chem. Phys. Lett., **93**, 74.

Törring, T. 1964, Z. Naturforsch., **19a**, 1426.

Törring, T., and Herrmann, R. 1989, Mol. Phys., **68**, 1379.

West, J.B., Bradford Jr., R.S., Eversole, J.D., and Jones, C.R.
1975, Rev. Sci. Instrum., **46**,164.

Winnewisser, M. 1981, Faraday Discuss. Chem. Soc., **71**, 31.

Yamada, C., Cohen, E.A., Fujitake, M., and Hirota, E. 1990b, J. Chem. Phys., **92**, 2146.

Yamada, C., Fujitake, M., and Hirota, E. 1989a, J. Chem. Phys., **91**, 137.

Yamada, C., Fujitake, M., and Hirota, E. 1989b, J. Chem. Phys., **90**, 3033.

Yamada, C., Fujitake, M., and Hirota, E. 1990a,

20 th International symposium on free radicals, Susono, Japan.

Yamamoto, S., and Saito, S. 1988, J. Chem. Phys., **89**, 1936.

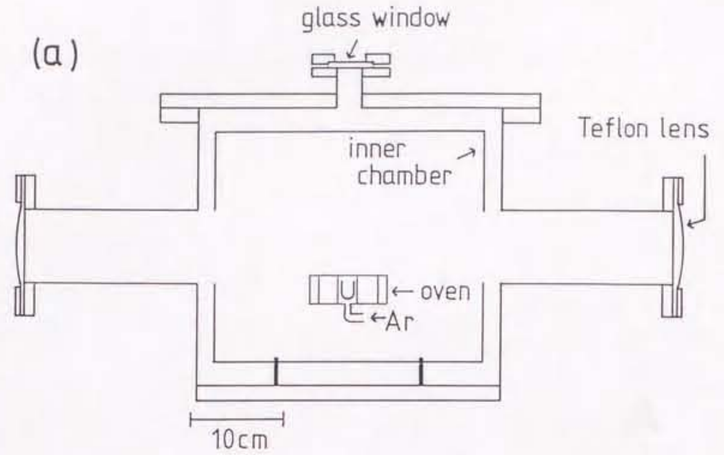

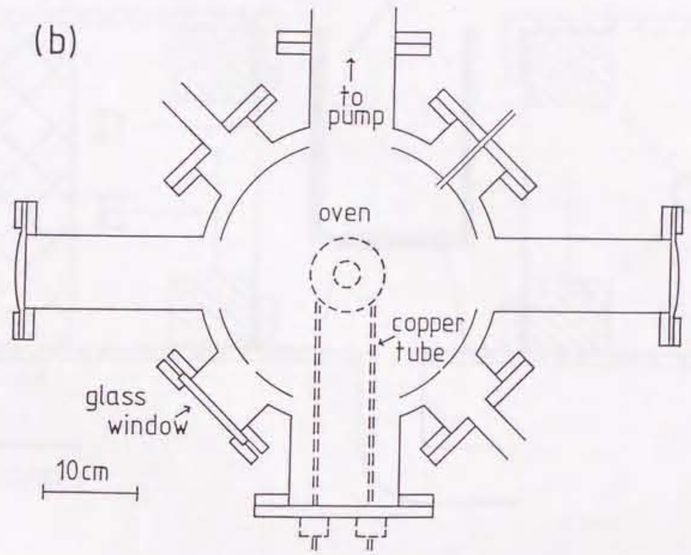

Figure 1: (a) Schematic cross section of the stainless steel chamber (high-temperature absorption cell) in a vertical plane including a pair of facing ports for microwave transmission. (b) Schematic cross section of the stainless steel chamber in a horizontal plane at the ports.

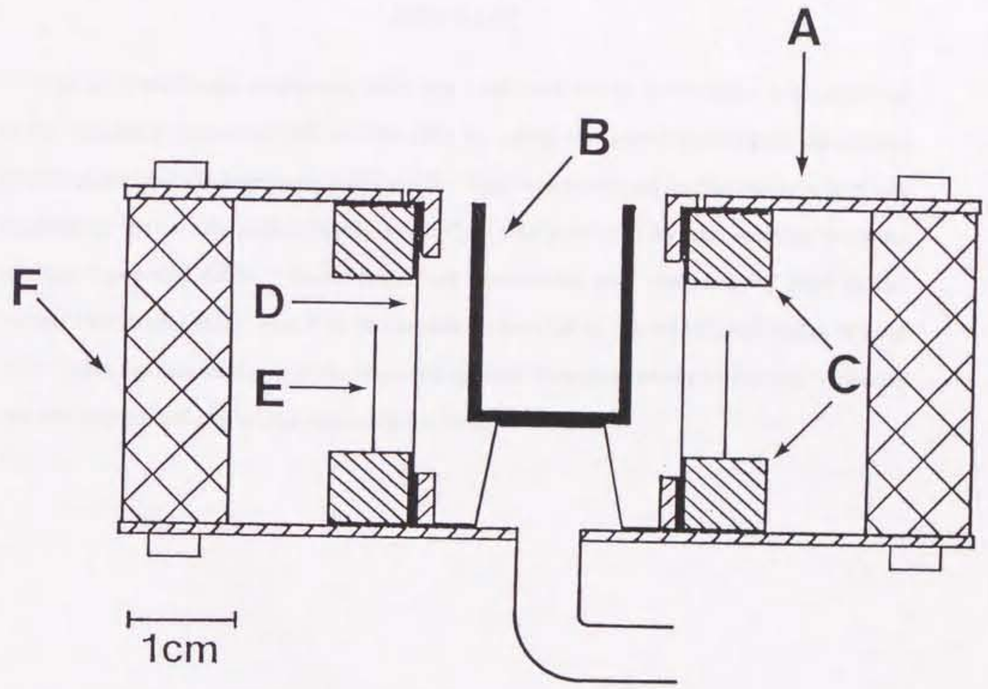

Figure 2: Schematic drawing of the oven. A– Stainless steel radiation shield, B– crucible, C– ring shaped Cu electrodes, D– Ta foil (heater), E– Ta radiation shield, F– ceramic spacers.

Chapter 3. Millimeter-Wave Spectra of Metal Sulfides

3-1. Millimeter-Wave Spectra of MgS and CaS

ABSTRACT

The pure rotational spectra of MgS and CaS both in the $X^1\Sigma^+$ state were observed in the frequency region of 200 to 300 GHz by using the source-modulated microwave spectrometer and the high-temperature cell. MgS was produced by the reaction between magnesium vapor and sulfur vapor, while CaS was produced by the reaction between calcium vapor and OCS. Seven rotational transitions were observed for MgS in the ground vibrational state, and 8 to 10 transitions for CaS in the vibrational states of v =0 to 3. Least-squares analyses of the observed spectral lines yielded the rotational constants and the centrifugal distortion constants for both molecules.

3-1-1. Introduction

Recently four metal halides, NaCl, AlCl, AlF and KCl, have been detected toward the red giant star IRC+10216 (Cernicharo and Guélin 1987). This suggests the possibility that molecules bearing low cosmic abundance atoms may be found in circumstellar envelopes or molecular clouds. Since the cosmic abundances of Mg and Ca are comparable with those of Si and Al, respectively, molecules containing Mg and Ca might be detectable in interstellar space. Their oxides, MgO (Turner and Steimle 1985; Miller et al. 1987) and CaO (Hocking et al. 1979), have been searched for toward stars and molecular clouds, but neither of them have been detected. According to the chemical equilibrium model proposed by Tsuji (1973), MgS and CaS have higher abundances than those of the corresponding oxides under certain conditions in stellar atmospheres (see Figure 2 and 3 in Chapter 1-1 of the present thesis). Since the molecular constants of CaS (Blues and Barrow 1969) and MgS (Marcano and Barrow 1970) have been known only from high-resolution optical spectroscopy, the author studied the pure rotational spectra of these molecules by microwave spectroscopy, aiming at determination of their accurate transition frequencies which may be useful for searches of interstellar and circumstellar MgS and CaS. In this section, the laboratory observation of the millimeter-wave spectra of MgS and CaS is reported.

3-1-2. Experimental

Details of the spectrometer used was given in a previous paper (Yamamoto and Saito 1988). The details of the high-temperature absorption cell used in this study were already described in Chapter 2. In short, the absorption cell is a cylindrical vacuum chamber of 40 cm in inner diameter and 30 cm in height, equipped with an oven bearing a crucible to produce the metal vapor.

MgS was produced by the reaction of magnesium vapor with sulfur vapor. The

magnesium vapor was produced by heating a magnesium metal ribbon in the carbon crucible to its melting point, and the sulfur vapor was produced by heating sulfur powder in a glass tube (Figure 1). No line was observed when OCS alone was added to magnesium vapor. The spectral line of MgS became stronger when argon was introduced in the chamber as a buffer gas. The optimum pressure of the gas was about 10 mTorr (which corresponds to 1.3 Pa). This fact indicates that the third body is effective for the production of MgS or for the retardation of the reactivity of MgS.

CaS was produced by the reaction of calcium vapor with OCS of about 10 mTorr. White chemiluminescence was clearly recognized in this reaction. A stainless steel crucible was used instead of the carbon crucible to produce calcium vapor by heating to its melting point, since calcium reacts with solid carbon. The lines were also observed when CS_2 or H_2S was introduced instead of OCS, but the line intensity was much weaker. The spectral line intensity of CaS was so strong that the rotational lines were observed for four vibrational states, from v =0 to 3. A typical signal to noise ratio was about 100 for the transition of J =26–25 in the ground vibrational state at 275 GHz. The spectral line intensity becomes weaker by about one half or one third as the vibrational quantum number increases by one. The intensity behavior with the vibrational quantum number suggests that the effective vibrational temperature of CaS is 600 ~ 900 K.

3-1-3. Results and Discussion

Seven rotational transitions of MgS in the ground vibrational state were observed in the frequency region of 224 ~ 368 GHz, as listed in Table 1. An example of the spectral lines observed is shown in Figure 2. The rotational constant and the centrifugal distortion constant were determined from the observed spectral lines by a least-squares method. The standard deviation of the fit was 0.014 MHz. The molecular constants determined are given in Table 2. The molecular constants agree with those obtained from the electronic absorption spectrum (Marcano and Barrow 1970), but the accuracy

of the constants has been improved by two orders of magnitude.

Eight to ten rotational transitions of CaS in the region of 198 ~ 306 GHz were observed for each vibrational state, as listed in Table 3. An example of the spectral lines observed is shown in Figure 3. The rotational constants and the centrifugal distortion constants determined by least-squares fits are shown in Table 2. The standard deviations of the fits are 0.017, 0.025, 0.018 and 0.030 MHz for the v =0, 1, 2 and 3 states, respectively. They also agree well with those obtained from the electronic absorption spectrum (Blues and Barrow 1969).

The rotational constant B_v is expressed in the power series expansion of $(v + 1/2)$. A least-squares fit of the rotational constants for CaS gave the equilibrium rotational constant and the vibration-rotation constants to be B_e=5296.6032(15), α_e=24.7921(22), and γ_e=−0.06959(60) MHz where the values in parentheses are three times the standard deviations of the fit. The equilibrium internuclear distance of CaS was derived to be 2.317751(1) Å. The error given in parentheses originates mainly from the errors in the equilibrium rotational constant and the fundamental physical constants. The small contribution of electrons to the moment of inertia was not included in the calculation.

The four centrifugal distortion constants were also fitted to the power series expansion of $(v + 1/2)$ as

$$D_v/MHz = 0.00309391(18) + 0.00001644(26) \times (v + 1/2) - 0.000000149(71) \times (v + 1/2)^2. \quad (1)$$

The first term is D_e, and the coefficient of the second term β_e. The vibrational frequency ω_e and the anharmonicity constant $\omega_e x_e$ were calculated to be 462.3 and 1.634 cm^{-1}, respectively, from B_e, D_e, and α_e (Gordy and Cook 1984). They are consistent with those obtained from the electronic absorption spectrum (Blues and Barrow 1969).

MgS could not be observed by the reaction of magnesium vapor with OCS. The heat of reaction of Mg + OCS ⟶ MgS + CO in the gas phase is estimated to be endothermic by more than 80 kJ mol^{-1}. On the other hand, the reaction of magnesium vapor with S_2 is exothermic. The heat of the three-body reaction 2Mg + S_2 ⟶ 2MgS in the gas

phase is estimated to be exothermic by less than 38 kJ mol^{-1}. For CaS, which was readily produced by the reaction of calcium vapor with OCS, the heat of reaction is also estimated to be exothermic by about 23 kJ mol^{-1}. Therefore, these exothermic reactions are considered to be effective for the production of MgS and CaS. The heat of reaction (23 kJ mol^{-1}) to produce CaS is considered to be sufficient to excite the vibration.

Mg and Ca isotopic species (^{25}MgS 10.00 %, ^{26}MgS 11.01 %, and ^{44}CaS 2.09 %) were not searched for because of the insufficient intensity of the normal species.

The molecular constants obtained in the present study enabled us to calculate the frequencies of low J transitions with an accuracy sufficient for the radioastronomical search for MgS and CaS. The spectral data toward relatively warm sources, our galactic center Sgr B2, the red giant star IRC+10216, and the massive star forming region W51A (Kaifu 1988) for MgS (J =7–6), and IRC+10216 (Cernicharo et al. 1987) for CaS (J =7–6) were examined at the relevant frequencies calculated. However no lines corresponding to the transitions of MgS or CaS were found above the signal to noise ratio levels attained at present. The details will be reported in Chapter 4.

REFERENCES

Blues, R.C., and Barrow, R.F. 1969, Trans. Faraday Soc., **65**, 646.

Cernicharo, J., and Guélin, M. 1987, Astron. Astrophys., **183**, L10.

Cernicharo, J., Kahane, C., Gómez-González, J., and Guélin, M. 1986, Astron. Astrophys., **164**, L1.

Gordy, W., and Cook, R.L. 1984, Microwave molecular spectra, 3rd edition (Wiley-Interscience, New York) Chapter 4.

Hocking, W.H., Winnewisser, G., Churchwell E., and Percival J. 1979, Astron. Astrophys., **75**, 268.

Kaifu, N. 1988, private communication.

Marcano, M., and Barrow, R.F., 1970, Trans. Faraday Soc., **66**, 2936.

Millar, T.J., and Elldér, J., Hjalmarson, Å, and Olofsson H. 1987, Astron. Astrophys., **182**, 143.

Tsuji, T. 1973, Astron. Astrophys., **23**, 411.

Turner, B.E., and Steimle, T.C. 1985, Astrophys. J., **299**, 956.

Yamamoto, S., and Saito, S. 1988, J. Chem. Phys., **89**, 1936.

TABLE 1
Observed transition frequencies of MgS ($v = 0$)[a].

Transition	ν_{obs}	$\Delta\nu$[b]
J =14–13	224103.178(45)[c]	0.019
16–15	256086.116(19)	-0.006
17–16	272072.920(29)	-0.017
18–17	288056.376(26)	0.000
19–18	304036.237(29)	-0.003
22–21	351952.415(30)	0.015
23–22	367915.973(43)	-0.007

[a]In MHz.
[b]$\Delta\nu = \nu_{obs} - \nu_{calc}$.
[c]The values in parentheses are one standard deviation of the frequency measurements and apply to the last digits of the frequencies.

TABLE 2
Molecular constants of MgS and CaS[a].

			MW[b]	Optical
MgS	$v=0$	B_0	8006.9278(15)	8007.25(39)[c]
		D_0	0.0082744(19)	0.008280(30)[c]
CaS	$v=0$	B_0	5284.1898(15)	5283.87(18)[d]
		D_0	0.0031021(11)	0.003058(12)[d]
		H_0	——	$-1.01(20)\times10^{-9}$ [d]
	$v=1$	B_1	5259.2581(21)	5258.66(24)[d]
		D_1	0.0031182(16)	0.0030609(90)[d]
		H_1	——	$-1.271(75)\times10^{-9}$ [d]
	$v=2$	B_2	5234.1881(18)	5233.69(33)[d]
		D_2	0.0031341(14)	0.003067(30)[d]
		H_2	——	$-1.66(75)\times10^{-9}$ [d]
	$v=3$	B_3	5208.9781(29)	——
		D_3	0.0031496(22)	——

[a]In MHz. The values in parentheses are three standard deviations and apply to the last digits of the constants.
[b]This study.
[c]Marcano and Barrow 1970. The values, originally reported in cm^{-1}, are converted to MHz.
[d]Blues and Barrow 1969. The values, originally reported in cm^{-1}, are converted to MHz.

TABLE 3
Observed transition frequencies of CaS[a].

	$v=0$		$v=1$	
Transition	ν_{obs}	$\Delta\nu$[b]	ν_{obs}	$\Delta\nu$
J=19–18	200714.113(10)[c]	0.011	199766.240(11)	-0.018
20–19	211268.339(7)	0.015	210270.546(12)	0.003
22–21	232372.216(4)	-0.010	231274.549(12)	0.001
23–22	242921.774(6)	0.017	241774.136(7)	0.018
24–23	253469.569(14)	-0.007	252271.978(18)	0.011
25–24	264015.580(29)	-0.028	262768.054(28)	0.034
26–25	274559.765(12)	-0.014	273262.163(13)	-0.039
27–26	285102.008(8)	-0.007	283754.405(18)	-0.033
28–27	295642.246(7)	0.006	294244.669(13)	0.015
29–28	306180.401(10)	0.021	304732.783(10)	0.009
	$v=2$		$v=3$	
Transition	ν_{obs}	$\Delta\nu$	ν_{obs}	$\Delta\nu$
J=19–18	198813.167(19)	0.005	197854.785(16)	0.030
20–19	209267.242(14)	0.008	——	
22–21	——		229060.893(37)	0.004
23–22	240620.142(35)	0.018	239459.704(33)	-0.004
24–23	251067.722(33)	-0.006	249856.794(23)	0.005
25–24	261513.512(43)	-0.014	260252.049(31)	-0.006
26–25	271957.413(10)	-0.031	270645.372(44)	-0.060
27–26	282399.408(32)	0.002	281036.828(25)	-0.015
28–27	——		291426.233(44)	0.019
29–28	303277.183(11)	0.020	301813.499(25)	0.031

[a]In MHz.
[b]$\Delta\nu = \nu_{obs} - \nu_{calc}$.
[c]The values in parentheses are one standard deviation of the frequency measurements and apply to the last digits of the frequencies.

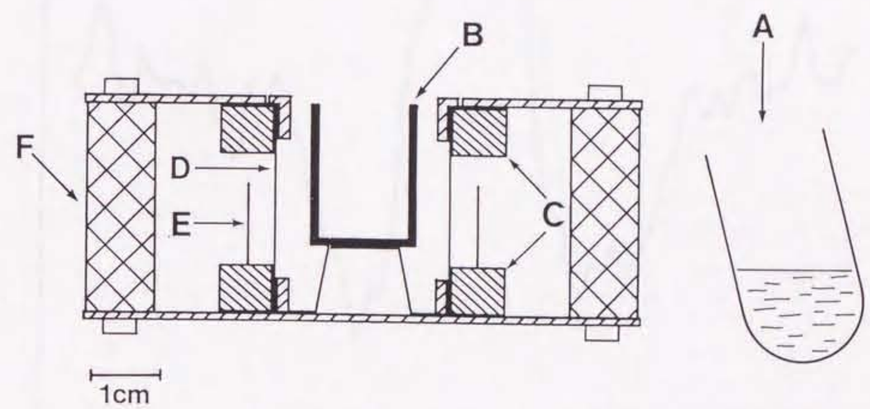

Figure 1: Schematic drawing of the oven and the glass tube to produce sulfur vapor. A– glass tube containing sulfur for MgS, B– crucible, C– ring shaped Cu electrodes, D– Ta foil (heater), E– Ta radiation shield, F– ceramic spacers.

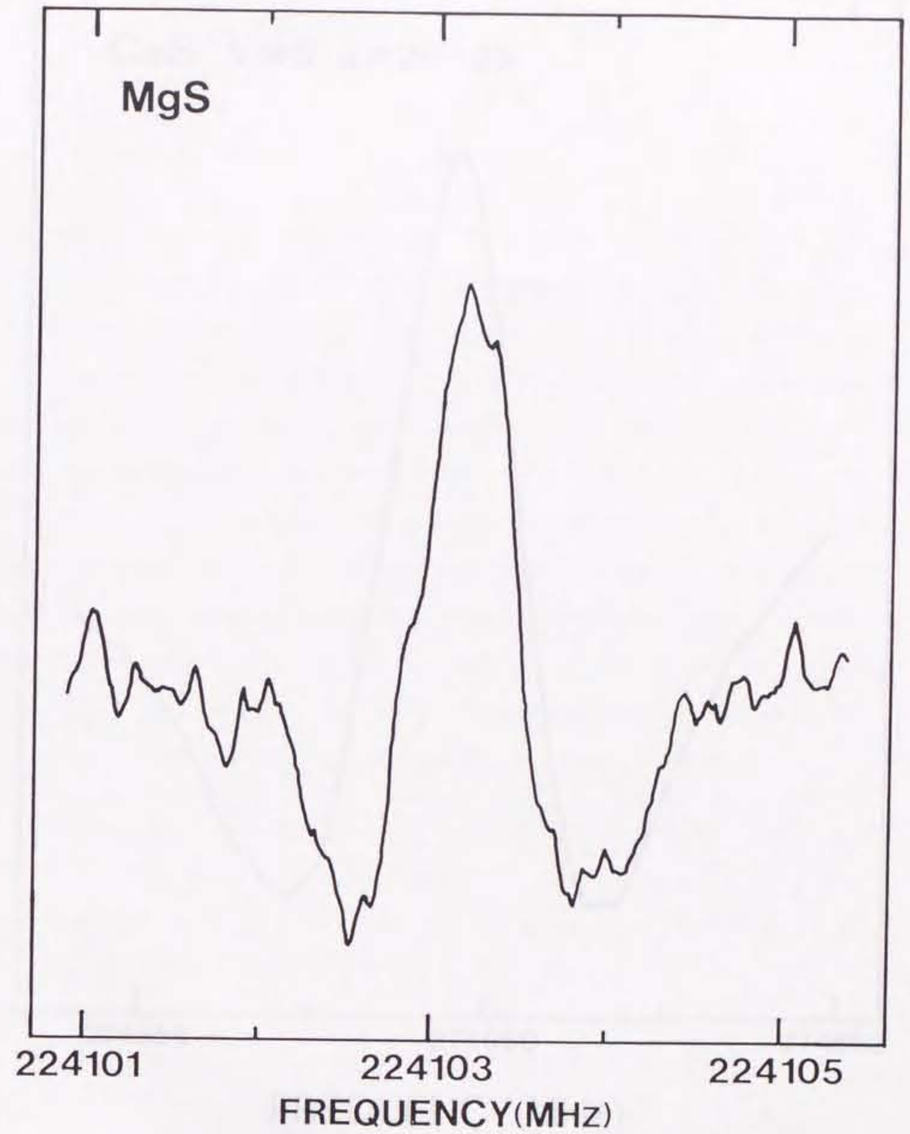

Figure 2: The $J = 14$–13 rotational spectral line of MgS. The integration time is about 25 seconds with PSD time constant of 1 ms.

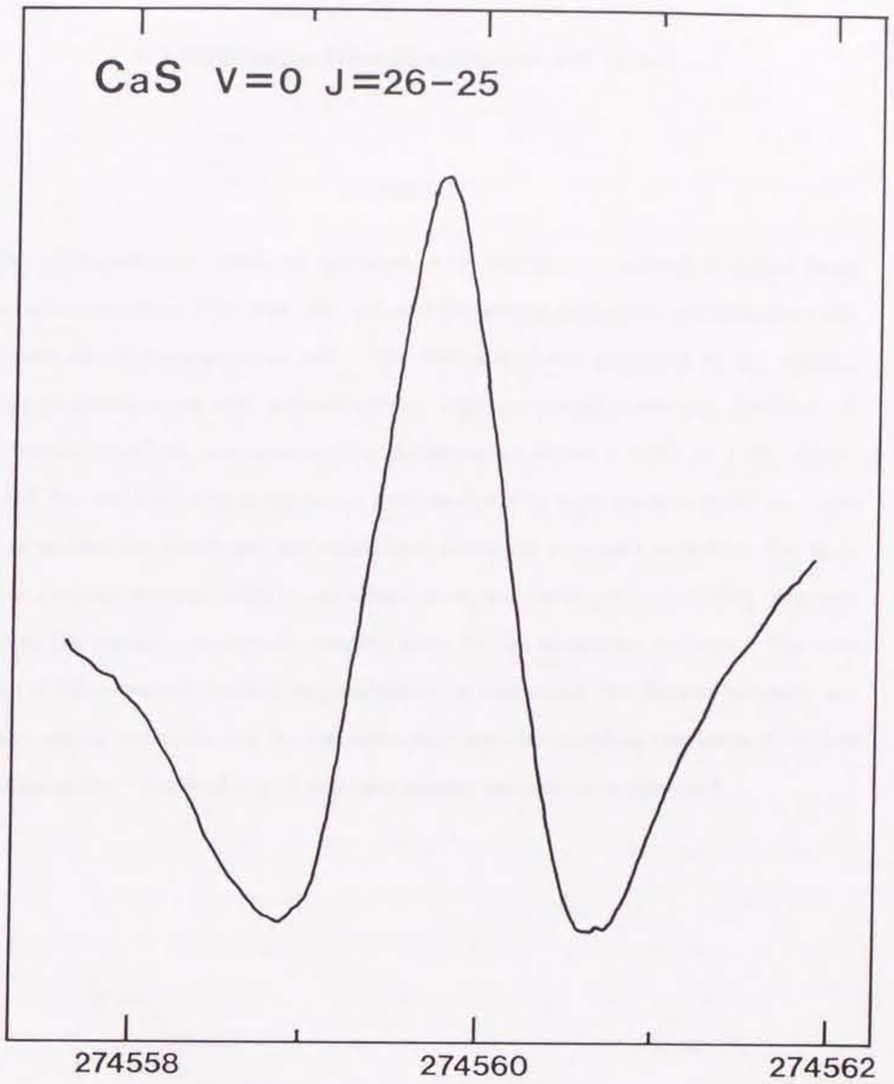

Figure 3: The $J = 26$–25 rotational spectral line of CaS in the ground vibrational state. The integration time is about 10 seconds with PSD time constant of 1 ms.

3-2. Millimeter-Wave Spectrum of AlS ($X^2\Sigma^+$)

ABSTRACT

The millimeter-wave rotational spectrum of the aluminum monosulfide radical in its ground electronic state $X^2\Sigma^+$ was observed with the source-modulated spectrometer combined with the high-temperature cell. The AlS radical was generated by the reaction between aluminum vapor and carbonyl sulfide. Eight rotational transitions, lowest N =4-3 and highest N =17-16, were measured in the frequency region of 67 to 284 GHz, and 75 observed fine and hyperfine components were analyzed by least-squares methods. The analysis yielded the rotational and centrifugal distortion constants as well as the spin-rotation coupling constant with its centrifugal term, and the hyperfine coupling constants including the nuclear quadrupole coupling term for the aluminum nucleus. The spin density of the unpaired electron was calculated by comparing the derived magnetic hyperfine coupling constants and the corresponding hyperfine coupling constants of the free aluminum atom. Applicability of this spin density calculation is discussed.

3-2-1. Introduction

The rotational spectra of the metal halides, NaCl, KCl, AlF, and AlCl, were recently detected by a radiotelescope in the envelope of the carbon star IRC+10216 (Cernicharo and Guélin 1987). Information on the interstellar abundances of such metal-containing molecules is useful for a deeper understanding of the physical and chemical processes in stellar envelopes and in hot interstellar regions. The metal halides were predicted to be relatively abundant in cool stellar atmospheres based on chemical equilibrium calculations for stellar atmospheric constituents (Tsuji 1973; see Figure 4 in Chapter 1-1 of the present thesis). According to this calculation, metal sulfides are also expected to have abundances similar to those of the metal halides. This suggests a possibility of radio astronomical detections of the metal sulfides. However, they have not been searched for in space, because their rotational transition frequencies have not been determined with sufficient accuracy for their identification in space. The laboratory study on the rotational spectra of MgS and CaS was already described in Chapter 3-1 (Takano, Yamamoto, and Saito 1989). In this section, the author reports the observation of the pure rotational spectrum of AlS ($X^2\Sigma^+$) by millimeter-wave spectroscopy in the laboratory. The analysis of the pure rotational spectrum yielded precise molecular constants including hyperfine coupling constants.

The electronic spectra of AlS have been extensively studied in the visible and ultraviolet regions (McKinney and Innes 1959; Maltsev, Shevelkov, and Krupnikov 1966; Kronekvist and Lagerqvist 1969; Lavendy, Mahieu, and Becart 1973; Lavendy and Jacquinot 1975; Lavendy 1980). McKinney and Innes (1959) first observed the emission spectrum of the $A^2\Sigma^+$-$X^2\Sigma^+$ system in the 3700-4800 Å region. They produced AlS in a graphite furnace containing aluminum and sulfur at 1800 °C, and determined several molecular constants including the rotational and centrifugal distortion constants in both of the electronic states. Lavendy, Mahieu, and Becart (1973) obtained the spin-rotation coupling constants in several vibrational levels of the $X^2\Sigma^+$ and $A^2\Sigma^+$ states. No ESR studies and

no ab initio calculations have been reported for AlS.

3-2-2. Experimental

The microwave spectrometer used was the 100 kHz source-modulated system (Yamamoto and Saito 1988) combined with the high-temperature absorption cell made of a cylindrical stainless steel chamber. The details of the high-temperature absorption cell were already described in Chapter 2.

The AlS radical was generated by a reaction between aluminum vapor and carbonyl sulfide. The aluminum vapor was produced by heating small pieces of aluminum metal in the alumina crucible of 1100-1300 °C. The temperature was measured by an optical pyrometer. The spectral lines of AlS were observed only when the temperature of the aluminum sample was considerably higher than its melting point (660 °C). Crucibles made of carbon or stainless steel could not be used because of their high reactivity with aluminum. The alumina crucible was also attacked slowly by aluminum. Argon at a pressure of about 5 mTorr was introduced from the bottom of the oven (Figure 1(a) in Chapter 2) as carrier gas and carbonyl sulfide was introduced over the oven as a source of sulfur. The optimum pressure of OCS for production of AlS was 5 to 10 mTorr. The absorption lines of AlS were easily observed with an oscilloscope display. The most probable reaction to generate AlS was Al + OCS $\longrightarrow$ AlS + CO. If the heat of formation of AlS is assumed to be 235 kJ mol^{-1} which is derived from the dissociation energy of AlS, 370 kJ mol^{-1} (Uy and Drowart 1971), the heat of reaction was estimated to be exothermic by about 60 kJ mol^{-1}. This high exothermicity may be responsible for the efficient production of AlS. The observed spectral lines of AlS were not so strong that the author did not try to observe the spectral lines in the vibrationally excited state.

The magnetic field generated by the current through the heater broadens the spectral lines of the radical. The Zeeman effects of high N transitions are generally small so that the spectral intensity shows little change with or without the current through the heater.

For low N transitions, however, the line broadening severely decreases the spectral line intensity. Hence the heater was turned off during data accumulation in the frequency measurements for low N transitions, below N =8-7. Eight rotational transitions, lowest N =4-3 and highest N =17-16, were measured in the 67 to 284 GHz region. Each rotational line splits into twelve main components by spin-rotation and hyperfine interaction due to the aluminum nucleus ($I = 5/2$). The observed spectral pattern of the N =17-16 transition is shown in Figure 1 as an example. In total, 81 fine and hyperfine components were measured and listed in Table 1. The frequencies were determined by the average of five up sweep and five down sweep measurements.

3-2-3. Analysis

The observed spectral lines were analyzed by using the Hamiltonian:

$$H = H_{rot} + H_{fs} + H_{hfs} + H_Q + H_{nsr} \quad , \tag{1}$$

where H_{rot} represents the rotational term including its centrifugal distortion effect, H_{fs} the spin-rotation interaction term (fine structure), H_{hfs} the magnetic hyperfine interaction term, H_Q the nuclear quadrupole interaction term, and H_{nsr} the nuclear spin-rotation interaction term for the aluminum nucleus. A preliminary analysis showed that the Fermi contact term is larger in energy than the spin-rotation interaction term. Hence Hund's coupling case $b_{\beta S}$ was used in the analysis. The matrix elements of the Hamiltonian were calculated with the coupling scheme of $I + S = F_2$ and $N + F_2 = F$ (Piltch et al. 1982; Bogey, Demuynck, and Destombes 1984; Tanimoto, Saito, and Hirota 1986; Törring and Hermann 1989), and the energy matrix was numerically diagonalized. The molecular constants were determined from the observed frequencies by least-squares methods. The standard deviation of the fit was 21 kHz, which is comparable to the experimental error. The molecular constants are listed in Table 2 and are compared with those derived from the electronic spectrum (Lavendy, Mahieu, and Becart 1973).

Most of the calculated transition frequencies below 300 GHz are listed in Table 1 for the convenience of astronomical observations. The line strength, S, and the energy of the upper state, E_{upper}, are also given in Table 1. The line strength was calculated by using the pure case $b_{\beta S}$ coupling scheme, since the mixing of other wavefunctions to the main wave function concerned turned out to be usually less than 10 %. The transitions having S larger than 1.0 were included in Table 1. The line strength of the transitions with $\Delta F = 0$ is significantly large in low N transitions.

3-2-4. Discussion

The rotational constant B_0 and the centrifugal distortion constant D_0 obtained in this study are in good agreement with those obtained from the electronic spectrum (Lavendy, Mahieu, and Becart 1973) (Table 2), but the accuracy of B_0 and D_0 is much improved in this study. The r_0 structure of AlS was calculated to be 2.031515(1) Å. The error given in parentheses originates from the errors in the rotational constant and fundamental physical constants. The harmonic vibrational frequency was calculated to be 613.0 cm^{-1} by using the formula $\omega = (4B^3/D)^{1/2}$. This value is consistent with the harmonic vibrational frequency ω_e derived from the electronic spectrum, 617.12 cm^{-1} (McKinney and Innes 1959). On the other hand, the spin-rotation coupling constant γ determined differs markedly from that obtained from the electronic spectrum (Lavendy, Mahieu, and Becart 1973). The discrepancy is beyond the error limits of both the studies. A similar discrepancy was reported for AlO (Yamada et al. 1990; Törring and Hermann 1989).

The s and p characters of the unpaired electron orbital on an atom in molecules have been calculated by comparing the observed hyperfine coupling constants with the corresponding free atomic values reported by Morton and Preston (1978) (free atom comparison method). The author compared the derived $b+c/3$ value of AlS with the isotropic hyperfine coupling constant (A_{iso}) of the free aluminum atom, 3911 MHz, and obtained 21 % for the s character. In order to obtain the p character, the derived $(5/6)c$ was compared

with the anisotropic hyperfine coupling constant (A_{dip}) of the free aluminum atom, 207.7 MHz, and 68 % was obtained for the p character. The p character was calculated on the assumption of $c = (6/5)g_S\beta g_N\beta_N < 1/r^3 >_S$ (the angular part is replaced by 4/5 for a p_σ orbital). The total spin density is 89 %. The result is listed in Table 3 with the results of related molecules AlO (Yamada et al. 1990), BO (Tanimoto, Saito, and Hirota 1986), and BS (Tanimoto, Saito, and Yamamoto 1988). Table 3 shows almost no differences in the s and p characters obtained from the free atom comparison method between AlO and AlS, and significant differences between BO and BS.

Knight et al. (1985) claimed that the percentages derived from the free atom comparison method do not always give the true values of the s and p characters for a series of isovalent molecules such as BO, CO^+, AlO, and SiO^+. They pointed out that the s and p characters calculated by the free atom comparison method do not necessarily coincide with those calculated by the Mulliken gross population analysis. The Mulliken gross population analysis is based on the ab initio CI wavefunctions which have good quality to reproduce the experimentally obtained hyperfine coupling constants. They found that the discrepancy between the two methods originates from the neglect of the large inner-shell contribution to the hyperfine coupling constants in the free atom comparison method. This inner-shell contribution becomes important for the heavier atoms contained in the molecule. For AlO and SiO^+, they found that there are large negative contributions from the inner s shells to the Fermi contact term and also significantly positive inner-shell contributions to the dipole-dipole interaction term. Since AlS is isovalent with AlO and SiO^+, the usual free atom comparison method is not valid for the determination of the s and p characters from experimental data of AlS. Table 3 shows that the s and p characters for BO determined by the free atom comparison method roughly correspond with those obtained from the Mulliken gross population analysis based on the ab initio CI wavefunctions. On the other hand, the s and p characters for AlO by the free atom comparison method are completely different from those from the Mulliken gross

population analysis. Referring to these facts, it is suggested that the near equality of the s and p characters between AlO and AlS by the free atom comparison method may be due to accidental balances between the real orbital characters and the inner-shell effects. Further quantitative discussions on the individual s and p characters of AlS could be made on the basis of a result from ab initio calculations.

The nuclear spin-rotation coupling constant C_I turned out to be very small and marginal, 0.0066(58) MHz, but the inclusion of this small term slightly improved the least-squares fitting. If the $B^2\Pi$ electronic state alone contributes to the constant, C_I is calculated to be 0.004 MHz with a second order perturbation method.

The AlS radical was searched for in IRC+10216 and other astronomical sources with the 45 m radiotelescope at Nobeyama Radio Observatory (Takano et al. 1990), but the author could not identify any features due to the lines of AlS. The details will be reported in Chapter 4.

REFERENCES

Bogey, M., Demuynck, C., and Destombes, J.L. 1984, Can. J. Phys., **62**, 248.

Cernicharo, J., and Guélin, M. 1987, Astron. Astrophys., **183**, L10.

Knight, L.B.Jr., Ligon, A., Woodward, R.W., Feller, D., and Davidson, E.R. 1985, J. Am. Chem. Soc., **107**, 2857.

Kronekvist M., and Lagerqvist, A. 1969, Arkiv för Fysik, **39**, 133.

Lavendy, H. 1980, J. Phys. B, **13**, 1151.

Lavendy, H., and Jacquinot, D. 1975, Can. J. Spectrosc., **20**, 141.

Lavendy, H., Mahieu, J.M., and Becart, M. 1973, Can. J. Spectrosc., **18**, 13.

Maltsev, A.A., Shevelkov, V.F., and Krupnikov, E.D. 1966, Optics and Spectrosc. Supplement, **2**, 4.

McKinney, C.N., and Innes, K.K. 1959, J. Mol. Spectrosc., **3**, 235.

Morton, J.R., and Preston, K.F. 1978, J. Magn. Reson., **30**, 577.

Piltch, N.D., Szanto, P.G., Anderson, T.G., Gudeman, C.S., Dixon, T.A., and Woods, R.C. 1982, J. Chem. Phys., **76**, 3385.

Takano, S. et al. 1990, unpublished.

Takano, S., Yamamoto, S., and Saito, S. 1989, Chem. Phys. Lett., **159**, 563.

Tanimoto, M., Saito, S., and Hirota, E. 1986, J. Chem. Phys., **84**, 1210.

Tanimoto, M., Saito, S., and Yamamoto, S. 1988, J. Chem. Phys., **88**, 2296.

Törring, T., and Hermann, R. 1989, Mol. Phys., **68**, 1379.

Tsuji, T. 1973, Astron. Astrophys., **23**, 441.

Uy, O.M., and Drowart, J. 1971, Trans. Faraday. Soc., **67**, 1293.

Yamada, C., Cohen, E.A., Fujitake, M., and Hirota, E. 1990, J. Chem. Phys., **92**, 2146.

Yamamoto, S., and Saito, S. 1988, J. Chem. Phys., **89**, 1936.

TABLE 1
Observed and calculated transition frequencies of the AlS radical ($^2\Sigma^+$).

N' - N	F_2	F' - F	ν_{obs}	$\Delta\nu^a$	S	E_{upper}
			MHz	kHz		cm^{-1}
4 - 3	3	7 - 6	66975.514(21)[b]	21	6.667	5.668
		6 - 5	(66961.441)[c]		5.056	5.668
		5 - 4	(66961.535)		3.714	5.667
		4 - 3	66964.861(19)	3	2.619	5.664
		3 - 2	(66963.712)		1.746	5.661
		2 - 1	(66951.743)		1.071	5.659
		5 - 5	(66920.108)		1.135	5.667
		4 - 4	(66889.331)		1.286	5.664
		3 - 3	(66878.278)		1.222	5.661
	2	6 - 5	(66925.435)		5.778	5.581
		5 - 4	66936.150(20)	16	4.400	5.581
		4 - 3	66939.861(30)	29	3.274	5.583
		3 - 2	(66945.236)		2.381	5.585
		2 - 1	(66959.312)		1.714	5.588
5 - 4	3	8 - 7	(83712.113)		7.727	8.460
		7 - 6	(83699.766)		6.234	8.460
		6 - 5	(83695.601)		4.949	8.459
		5 - 4	(83693.452)		3.861	8.456
		4 - 3	(83688.691)		2.955	8.453
		3 - 2	(83677.162)		2.222	8.450
		2 - 1	(83655.452)		1.667	8.447
		5 - 5	(83621.248)		1.089	8.456
		4 - 4	(83602.110)		1.064	8.453
	2	7 - 6	(83659.842)		6.818	8.371
		6 - 5	(83669.903)		5.515	8.372
		5 - 4	(83676.038)		4.412	8.374
		4 - 3	(83683.456)		3.500	8.377
		3 - 2	(83696.705)		2.778	8.380
6 - 5	3	9 - 8	100447.412(17)	20	8.769	11.811
		8 - 7	100436.229(26)	7	7.356	11.810
		7 - 6	100430.369(6)	26	6.114	11.809
		6 - 5	100425.739(14)	-14	5.035	11.806
		5 - 4	(100419.239)		4.112	11.803
		4 - 3	100407.633(12)	-7	3.341	11.799
		3 - 2	100387.672(10)	-34	2.727	11.795
	2	8 - 7	100393.680(8)	5	7.846	11.720
		7 - 6	100403.255(12)	-1	6.593	11.721
		6 - 5	100410.447(8)	24	5.507	11.723
		5 - 4	(100418.769)		4.582	11.726
		4 - 3	100431.735(37)	4	3.818	11.730
8 - 7	3	11 - 10	133914.054(17)	-26	10.824	20.186
		10 - 9	133904.477(9)	-33	9.512	20.185
		9 - 8	133897.416(19)[d]	-126	8.327	20.183
		8 - 7	133891.032(9)	-1	7.265	20.180
		7 - 6	133883.013(5)	20	6.323	20.176
		6 - 5	133871.052(21)	2	5.500	20.172
		5 - 4	(133851.740)[e]		4.800	20.167
	2	10 - 9	133858.577(18)	1	9.882	20.092
		9 - 8	133867.377(10)	-7	8.693	20.094
		8 - 7	133875.246(12)	18	7.628	20.096
		7 - 6	133884.369(28)[f]	70	6.686	20.100
		6 - 5	133897.416(19)[d]	291	5.867	20.104

continued

N' - N	F_2	F' - F	ν_{obs}	$\Delta\nu^a$	S	E_{upper}
			MHz	kHz		cm^{-1}
9 - 8	3	12 - 11	(150645.327)		11.842	25.211
		11 - 10	(150636.353)		10.565	25.210
		10 - 9	(150629.279)		9.399	25.207
		9 - 8	(150622.409)		8.344	25.204
		8 - 7	(150614.046)		7.396	25.200
		7 - 6	(150601.961)		6.555	25.195
		6 - 5	(150582.370)		5.824	25.190
	2	11 - 10	(150589.230)		10.895	25.115
		10 - 9	(150597.698)		9.726	25.117
		9 - 8	(150605.595)		8.669	25.120
		8 - 7	(150614.775)		7.721	25.124
		7 - 6	(150627.588)		6.882	25.129
10 - 9	3	13 - 12	(167375.006)		12.857	30.794
		12 - 11	(167366.547)		11.607	30.793
		11 - 10	(167359.492)		10.458	30.790
		10 - 9	(167352.446)		9.408	30.786
		9 - 8	(167343.910)		8.454	30.782
		8 - 7	(167331.724)		7.599	30.777
		7 - 6	(167311.662)		6.842	30.771
	2	12 - 11	(167318.438)		11.905	30.696
		11 - 10	(167326.585)		10.753	30.698
		10 - 9	(167334.445)		9.702	30.702
		9 - 8	(167343.642)		8.749	30.706
		8 - 7	(167356.438)		7.895	30.711
11 - 10	3	14 - 13	184102.974(16)	4	13.870	36.935
		13 - 12	184094.970(9)	4	12.642	36.933
		12 - 11	184088.016(22)	14	11.506	36.931
		11 - 10	184080.914(23)	14	10.460	36.927
		10 - 9	184072.313(8)	18	9.503	36.922
		9 - 8	184060.063(12)	13	8.635	36.916
		8 - 7	184039.402(10)	11	7.857	36.909
	2	13 - 12	184046.040(18)	17	12.913	36.835
		12 - 11	184053.881(14)	17	11.775	36.838
		11 - 10	184061.630(21)	2	10.728	36.841
		10 - 9	184070.781(18)	2	9.771	36.846
		9 - 8	184083.547(17)	7	8.905	36.851
12 - 11	3	15 - 14	200829.025(15)	-41	14.880	43.634
		14 - 13	200821.444(25)	-26	13.671	43.632
		13 - 12	200814.607(12)	-36	12.547	43.629
		12 - 11	200807.548(8)	-13	11.504	43.625
		11 - 10	200798.959(3)	-5	10.544	43.620
		10 - 9	200786.830(9)[d]	126	9.665	43.614
		9 - 8	200765.324(16)	-32	8.870	43.606
	2	14 - 13	200771.829(7)	16	13.920	43.532
		13 - 12	200779.361(15)	2	12.794	43.535
		12 - 11	200786.830(9)[d]	-158	11.751	43.539
		11 - 10	200796.050(9)	5	10.791	43.544
		10 - 9	200808.746(9)	-0	9.913	43.550
13 - 12	3	16 - 15	217553.125(20)	-9	15.889	50.891
		15 - 14	217545.931(11)	21	14.696	50.889
		14 - 13	217539.242(30)	-4	13.581	50.885
		13 - 12	217532.097(7)[d]	-142	12.542	50.881

continued

N' - N	F_2	F' - F	ν_{obs}	$\Delta\nu^a$	S	E_{upper}
			MHz	kHz		cm^{-1}
13 - 12	3	12 - 11	217523.708(22)	3	11.579	50.876
		11 - 10	217511.494(13)	19	10.691	50.869
		10 - 9	217489.315(28)	-55	9.880	50.861
	2	15 - 14	217495.636(18)	1	14.926	50.787
		14 - 13	217502.879(16)	-20	13.810	50.790
		13 - 12	217510.348(8)	-18	12.770	50.794
		12 - 11	217519.296(14)	6	11.807	50.799
		11 - 10	217532.097(7)[d]	195	10.920	50.806
14 - 13	3	17 - 16	(234275.015)		16.897	58.706
		16 - 15	(234268.132)		15.718	58.703
		15 - 14	(234261.647)		14.610	58.699
		14 - 13	(234254.753)		13.574	58.695
		13 - 12	(234246.326)		12.608	58.689
		12 - 11	(234234.169)		11.713	58.683
		11 - 10	(234211.255)		10.889	58.673
	2	16 - 15	(234217.319)		15.931	58.600
		15 - 14	(234224.311)		14.823	58.603
		14 - 13	(234231.597)		13.786	58.607
		13 - 12	(234240.360)		12.821	58.613
		12 - 11	(234252.850)		11.926	58.620
15 - 14	3	18 - 17	(250994.544)		17.903	67.078
		17 - 16	(250987.977)		16.736	67.075
		16 - 15	(250981.681)		15.636	67.071
		15 - 14	(250974.926)		14.602	67.067
		14 - 13	(250966.641)		13.634	67.061
		13 - 12	(250954.600)		12.732	67.054
		12 - 11	(250930.836)		11.897	67.044
	2	17 - 16	(250936.698)		16.935	66.970
		16 - 15	(250943.427)		15.835	66.974
		15 - 14	(250950.519)		14.800	66.978
		14 - 13	(250959.096)		13.833	66.984
		13 - 12	(250971.431)		12.931	66.991
16 - 15	3	19 - 18	267711.522(35)	-37	18.909	76.008
		18 - 17	267705.286(35)	2	17.753	76.005
		17 - 16	267699.168(16)	-15	16.659	76.001
		16 - 15	267692.567(25)	-20	15.627	75.996
		15 - 14	267684.515(12)	44	14.657	75.990
		14 - 13	267672.624(14)	37	13.749	75.982
		13 - 12	267647.900(13)	-41	12.903	75.971
	2	18 - 17	267653.614(8)	13	17.939	75.898
		17 - 16	267660.102(17)	25	16.845	75.902
		16 - 15	(267666.967)[e]		15.813	75.907
		15 - 14	267675.349(36)	11	14.843	75.912
		14 - 13	267687.489(8)	7	13.935	75.920

continued

N' - N	F_2	F' - F	ν_{obs}	$\Delta\nu^a$	S	E_{upper}
			MHz	kHz		cm^{-1}
17 - 16	3	20 - 19	284425.891(21)	-3	19.914	85.495
		19 - 18	284419.896(21)	3	18.767	85.492
		18 - 17	284414.013(3)	25	17.678	85.488
		17 - 16	284407.575(31)	12	16.649	85.483
		16 - 15	284399.621(38)	-17	15.677	85.476
		15 - 14	284387.942(29)	-8	14.764	85.468
		14 - 13	284362.303(21)[f]	-96	13.909	85.457
	2	19 - 18	284367.841(9)	-20	18.943	85.384
		18 - 17	284374.091(28)	-3	17.854	85.388
		17 - 16	284380.869(36)[f]	94	16.824	85.392
		16 - 15	284388.935(36)	10	15.852	85.399
		15 - 14	284400.863(35)	18	14.939	85.407

[a] $\Delta\nu = \nu_{obs} - \nu_{calc}$.
[b] One standard deviation of the frequency measurement in kHz.
[c] The values in parentheses are the calculated frequencies using the molecular constants listed in Table 2.
[d] This line is blended with an other line of AlS (not used in the least-squares fitting).
[e] Disturbed, and the calculated frequency is given.
[f] Measured, but disturbed (not used in the least-squares fitting).

TABLE 2
Molecular constants of the AlS radical (in MHz).

	MW(This study) [a]	Optical[b]
B	8368.54400(85)	8367.
D	0.0069412(19)	0.0078
γ	66.051(57)	1.3×10^2
γ_D	−0.002169(91)	
$b+c/3$	819.9(12)	
c	169.37(78)	
C_I	0.0066(58)	
eQq	−24.2(25)	

[a] The values in parentheses are three standard deviations and apply to the last digits of the constants.
[b] Lavendy, Mahieu, and Becart 1973. The values, originally reported in cm^{-1}, are converted to MHz.

TABLE 3
The s and p characters of AlS and its related molecules (in %).

		AlS(This study)	AlO [a]	BS [b]	BO [c]
		Free Atom Comparison Method			
$(b+c/3)/A_{iso}$	(s character)	21	19	31	40
$(5/6)c/A_{dip}$	(p character)	68	68	49	43
total		89	87	80	83
		Mulliken Gross Population Analysis (ab initio) [d]			
s character		—	41	—	57
p character		—	26	—	39

[a] Calculated from the molecular constants listed in Yamada et al. 1990.
[b] Tanimoto, Saito, and Yamamoto 1988.
[c] Tanimoto, Saito, and Hirota 1986.
[d] Knight et al. 1985.

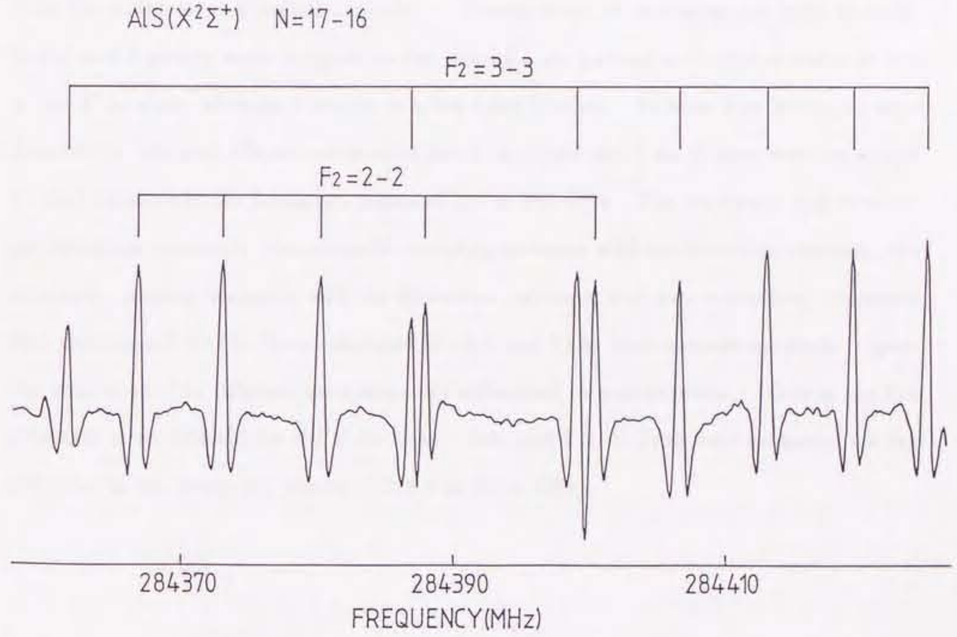

Figure 1: The N = 17-16 rotational spectral line of AlS in the 284 GHz region. The integration time is 27 seconds with PSD time constant of 1 ms. The spectral line splits into twelve fine and hyperfine components.

3-3. Millimeter-Wave Spectrum of FeS

ABSTRACT

The millimeter-wave rotational spectra of the iron monosulfide radical were observed by using the free space absorption cell combined with the source-modulated spectrometer. The FeS radical was efficiently generated in the free space absorption cell by the stainless steel hollow cathode discharge in a mixture of Ar and H_2S. The iron atom is supplied from the stainless steel hollow cathode. Eleven series of paramagnetic lines were detected and 6 groups were assigned to the vibrationally ground and excited states of FeS in the $X^5\Delta_i$ state, whereas 5 groups to a low lying Σ state. At least four substates were detected for the v=0 vibrational level of the $X^5\Delta_i$ state, and 5 to 15 lines were measured for each substate in the frequency region of 220 to 392 GHz. The rotational and centrifugal distortion constants, the spin-orbit coupling constant with its distortion constant, the spin–spin coupling constant with its distortion constant, and two Λ-doubling constants were determined for the three substates (Ω=4,3, and 1) by least-squares methods. Spectral lines in the $^5\Delta_2$ substate are apparently influenced by perturbation. Lines in the five substates were detected for the Σ electronic state and 5 to 15 lines were measured for the substates in the frequency region of 223.2 to 394.4 GHz.

3-3-1. Introduction

Iron is the heaviest product of the nuclear systheses in stars, and its cosmic abundance (5.94 in Table 2 in Chapter 1) is comparable to that of silicon (6.00 in Table 2 in Chapter 1). However, no molecules containing the iron atom have been identified in space. The rotational spectral lines of iron monoxide (FeO) have been searched for toward interstellar clouds and stars; only upper limits to the abundance of FeO have been obtained (Merer, Walmsley, and Churchwell 1982; Cernicharo and Guélin 1987). The iron atom is considered to be locked up in dust grains, but molecules containing the iron atom may exist in the gas phase in hot regions such as circumstellar envelopes and star forming regions. Tsuji (1973) predicted that FeS is more abundant than FeO in cool stellar atmospheres as shown in Figure 5 in Chapter 1. However, no searches have been carried out for FeS, because no spectroscopic data have been reported on FeS. In the case of the related molecule FeO, its ground electronic state was found to be $^5\Delta_i$ (Cheung, Gordon, and Merer 1981), although its electronic spectra show rather complicated and perturbed features. Furthermore, the existence of low lying Σ electronic states has been suggested for FeO (Engelking and Lineberger 1977; Taylor, Cheung, and Merer 1985; Kröckertskothen, Knöckel, Tiemann 1986). There is no spectroscopic data in any frequency region for FeS, and no information is available about the ground electronic state of FeS. According to the electronic structure of FeO, the ground electronic state of FeS is probably $^5\Delta_i$ and the Σ electronic states may exist at low energy above the ground electronic state. In this section, the author reports the millimeter-wave spectra of FeS in its two electronic states. Information about the electronic structure is obtained by analyzing the rotational spectra.

3-3-2. Experimental

The 100 kHz source-modulated microwave spectrometer (Yamamoto and Saito 1988)

was used with the 2 m long free space absorption cell. A mixture of Ar (or He) and H_2S (or OCS, CS_2) was discharged in the free space cell equipped with a 1.4 m long stainless steel hollow cathode. The iron atom was expected to be supplied from the stainless steel hollow cathode to the gas phase. Since no spectroscopic data and no theoretical calculations were reported for FeS, the rotational constant of FeS was estimated to be between 5.1 and 6.3 GHz from the molecular constants of the related molecules. Then, paramagnetic lines were searched for in a wide frequency range of more than 20 GHz. Consequently several series of paramagnetic lines were found as schematically shown in Figure 1. In this Figure, the frequency axis is shown with the intervals of 12 GHz, which is close to the intervals of the adjacent two lines in each series. This made it easy to pick up series of lines obeying to harmonic relations (Loomis-Wood diagram). The ordinate indicates the relative intensity. These intervals are close to the two times of the expected rotational constant of FeS. The lines indicated by closed circles show relatively large Zeeman effect. Two series showing doublet patterns were found as indicated in Figure 1. These doublings are considered to be Λ-doubling. In addition, the lines indicated by asterisks are not assigned to members of series lines, because only four successive lines were detected from J=28-27 to J=31-30, but the lines in the J=27-26 and J=32-31 transitions have not been detected near the predicted frequencies.

These paramagnetic lines show the following production behaviors. (1) The intensity decreases as oxygen is introduced in the cell. (2) The lines are observed by discharging Ar (He) with only a trace amount of H_2S (or OCS, CS_2). (3) The intensity decreases severely when the discharge current is decreased from 500 mA to 50 $\sim$ 100 mA. The optimum condition to give these lines is a 500 mA discharge in the mixture of 10 mTorr of Ar (or 20 mTorr of He) and 1 mTorr of H_2S (or OCS, CS_2). The intensity increases as the current increases, but 500 mA was adopted for stable discharge. The change in the temperature of the cell does not affect the production so much that the temperature was maintained between 190 to 270 K.

The series of the paramagnetic lines were not observed when an aluminum hollow cathode was used instead of the stainless steel one. Subsequently, ferrocene ($(C_5H_5)_2Fe$) was introduced into the cell and discharged with OCS with the aluminum hollow cathode. In this time the series of the paramagnetic lines were weakly reproduced. Therefore, the molecule contains the iron atom, and that the stainless steel hollow cathode actually supplies the iron atom to the gas phase.

Furthermore, the same series of the paramagnetic lines were observed by the reaction between iron vapor and CS_2 in the high-temperature absorption cell. The temperature of the oven was measured with an optical pyrometer and was found to be about 1700 K. At this temperature, iron in the alumina crucible melted completely. About 10 mTorr of CS_2 as a source of sulfur was introduced into the cell, whereas about 5 mTorr of Ar as carrier gas from the bottom of the oven (Figure 2 in Chapter 2). From these evidences, the author concluded that the carrier molecule of the series of paramagnetic lines is FeS.

An example of the spectral line is shown in Figure 2. This line belongs to one of series lines with the strongest intensity, and was clearly observed with an oscilloscope display.

3-3-3. Analysis

In order to make clear the characters of these series in detail, the frequencies of these lines were divided by the rotational quantum numbers of the upper levels, and the derived $2B_{eff}$ values were plotted against the rotational quantum numbers. In the case of the series except those indicated by closed circles in Figure 1, the change in the $2B_{eff}$ values can be fitted to a linear line. This result is shown in Figure 3(a). The frequencies of these lines are listed in Table 1. In the case of the five series indicated by closed circles in Figure 1, the change in the $2B_{eff}$ values could not be fitted to a linear line. This result is shown in Figure 3(b). The frequencies of lines which belong to these five series are listed in Table 2. Therefore, all of the series in Figure 1 were classified into two groups; series

with the linear behavior (Figure 3(a)) and series with the non-linear behavior (Figure 3(b)) against the rotational quantum number.

3-3-3-1. The Series of Lines in the $X^5\Delta_i$ State

At least seven series exist in Figure 3(a). Two of them with weaker intensity show Λ-doubling, and two series at lower frequency are considered to belong to the v=1 vibrational level from their weaker intensity. This fact means that these series are considered to belong to the orbitally degenerate electronic state with S (total electronic spin) greater than 2 and with a negative spin-orbit coupling constant; for example $^5\Pi_i$ or $^5\Delta_i$. The latter state is consistent with a prediction that the ground electronic state of FeS is $^5\Delta_i$, as the ground electronic state of FeO suggests. Therefore, these series were assigned to the v=0 and 1 vibrational levels of the $^5\Delta_i$ electronic state and the assigned Ω values were indicated in Figure 1 and 3(a). The assignment of the series indicated by squares in these Figures is not clear. One possibility is that this series belongs to one component of the Λ-doubling in the $^5\Delta_0$ substate. Since the v=0 level of the Ω=4 substate is strongest in the intensity, the $^5\Delta_i$ electronic state is considered to be the ground electronic state.

These spectral lines were analyzed using the matrix elements for the $^5\Delta$ state (Brown, Cheung, and Merer 1987) by least-squares methods. At first, the author tried to fit Ω=4, 3, and 2 substates simultaneously, but the systematic residuals of the spectral lines in Ω=2 substate were much larger than the experimental errors. Then, the Ω=1 substate was included in the least-squares fitting and a good fitting of the Ω=1 substate was obtained. However, the residuals of the Ω=2 lines were not improved significantly. The residuals in this fitting are shown in Table 1, and the constants determined are listed in Table 3. From the individual fitting of each group of lines to the formula, $\nu = 2B_{eff}(J+1) - 4D_{eff}(J+1)^3$, the D_{eff} value of the Ω=2 substate was found to be significantly smaller than those from the Ω=4, 3, and 1 substates as shown in Table 4. In this fitting, the average values of Λ-doubling components were used for the Ω=2 and Ω=1 substates. The residuals were large for the Ω=2 substate, but the Ω=1 substate was fitted well. The results of the

fitting were also listed for each Λ-doubling component in the Ω=1 substate. Based on these results, the author concluded that the Ω=2 substate is somewhat perturbed. The spectral lines of Ω=4 and 3 in the v=1 vibrational state were also analyzed by using the matrix elements for the $^5\Delta$ state by least-squares methods. Only B, D, and λ_D were employed as parameters, because of the limited number of the observed lines. The obtained constants are listed in Table 3, and the residuals are listed in Table 1.

Two series of the ground vibronic state, $^5\Delta_2$ and $^5\Delta_1$, appeared as doublets. The frequency separations in each doublet increase as the rotational quantum number (J) increases, and the J dependence of the doublet gives valuable information on the assignment of the Ω substates, because its dependence is roughly determined by the quantum number Ω. In Figure 4(a), the frequency separations of the $^5\Delta_2$ substate were plotted against the rotational quantum number. The separation increases rapidly as the rotational quantum number increases. In Figure 4(b), both axes are the same as Figure 4(a), but the scale is given by logarithm, and the separations were found to be proportional to roughly J^4. The similar plot for the $^5\Delta_1$ substate was shown in Figure 5. The separations were found to be proportional to roughly $J^{1.5}$. Brown, Cheung, and Merer (1987) discussed the J dependence of the Λ-doubling separation by reffering to the matrix elements for the Δ state in Hund's case(a) coupling scheme. According to their results, the observed separation of the Λ-doubling is proportional to roughly $[J(J+1)]^{\Omega}/J \sim J^{2\Omega-1}$. From the J dependence obtained in the present measurements, the Ω values were calculated to be 2.5 and 1.25 for $^5\Delta_2$ and $^5\Delta_1$ states, respectively. This result is consistent with the earlier assignment of these doublet series to the substates, $^5\Delta_2$ and $^5\Delta_1$, and is another evidence supporting that the ground electronic state of FeS is $^5\Delta_i$.

The Zeeman effect of each substate in the $^5\Delta_i$ electronic state in the v=0 and 1 vibrational states was measured, and the result is shown in Figure 6(a) and 6(b), respectively. Since the M_J components were not resolved, the full line width at the half maximum intensity was measured at several values of the magnetic fields. As shown in Figure 6(a),

the Zeeman effect becomes small as the Ω value decreases from 4 to 2, but the Zeeman effect unexpectedly increases in the Ω=1 substate. In case(a) limit, the $^5\Delta_1$ substate does not have the Zeeman effect. Therefore, the relatively large Zeeman effect in the $^5\Delta_1$ substate suggests that the $^5\Delta_i$ electronic state of FeS is in intermediate coupling between case(a) and case(b) in these high J transitions. The result of the Zeeman effect in the v=1 state (Figure 6(b)) is similar to that of the corresponding substates in the v=0 state. This similarity confirms the assignment of the v=1 substates.

3-3-3-2. The Series of Lines in the Low Lying Σ State

All of the five series indicated by closed circles in Figure 1 show non-linear $2B_{eff}$ behavior (Figure 3(b)), and this suggests that these series belong to the Σ electronic state with S larger than 2; for example $^5\Sigma$ or $^7\Sigma$. This non-linear behavior seems to originate from a transition from case(a) to case(b) as the rotational quantum number (N) increases.

The Zeeman effect of these series is relatively much larger than that of the $^5\Delta_i$ substates as shown in Figure 7. The large Zeeman effect is another evidence suggesting that these lines belong to the Σ electronic state. Therefore, the existence of the low lying Σ electronic state was definitely shown.

3-3-4. Discussion

3-3-4-1. The $X^5\Delta_i$ Electronic State

From the obtained B_0 value listed in Table 3, the r_0 structure was calculated to be 2.0170163(22) Å. The error in parentheses originates mainly from errors of the rotational constant and fundamental physical constants. The vibrational frequency was calculated to be 506.3 cm^{-1} by using the formula $\omega = (4B_0^3/D_0)^{1/2}$. Generally, it is difficult to determine the spin-orbit coupling constant with pure rotational spectroscopy. The A_{SO}

value was fixed to –3000000 MHz (~ –100 cm^{-1}). However, the spectral lines in the v=0 vibrational level could not be fitted well by fixing the A_{SO} value to –3000000 MHz. Then, the A_{SO} value was employed as a parameter and determined to be –1339974(6000) MHz (=–44.7 cm^{-1}). This value is smaller than the A_{SO} value of FeO ($X^5\Delta_i$), –94.9462(22) cm^{-1} (Taylor, Cheung, and Merer 1985). Usually, the A_{SO} values of sulfides are larger than those of the corresponding oxides. For example, the A_{SO} value of PO is 224.01 cm^{-1} (Verma and Singhal 1975) and PS is 321.93 cm^{-1} (Narasimham and Balasubramanian 1971). The result may indicate that there is the effect of perturbation not only in the $^5\Delta_2$ substates, but also slightly in the $^5\Delta_1$ substate. In the v=1 vibrational level, the lines in the $^5\Delta_4$ and $^5\Delta_3$ substates were fitted well with the fixed A_{SO} value. Therefore, the effect of perturbation seems small for the $^5\Delta_4$ and $^5\Delta_3$ sublevels.

This local perturbation was probably caused by another electronic state which exists near the $^5\Delta_2$ substate in energy. The low lying Σ electronic state is the most likely candidate for the perturbing state. The Δ and Σ electronic states interact through the spin-spin interaction. Since one of the selection rules of the spin-spin interaction is $\Delta\Omega$=0, the low lying $^5\Sigma$ or $^7\Sigma$ state can interact at least with the $^5\Delta_2$ and $^5\Delta_1$ substates. At present, informaiton on the excited electronic states is limited, and the detailed analysis of the perturbation remains as a future problem.

3-3-4-2. The Low Lying Σ Electronic State

At present, five series were detected. If these series belong to the Σ electronic state as discussed above, the Zeeman effect of one of the series must be relatively small by a factor of N in case (b) limit. However, as shown in Figure 7, there is no such large difference in the Zeeman effect. This means that the Σ electronic substates have not been detected completely at present. Low lying Σ electronic states have been suggested for FeO as written in the introduction of this section. Engelking and Lineberger (1977) reported the low lying (3990±100 cm^{-1} above the ground state) $^5\Sigma$ electronic state from the laser photoelectron spectroscopy of FeO^- and the ab initio calculations. Furthermore, Taylor,

Cheung, and Merer (1985) suggested the existence of the low lying (2100 cm^{-1} above the ground state) $^7\Sigma$ electronic state from the analysis of the perturbation and the ab initio calculation. Since another series was expected for the low lying Σ electronic state of FeS (in addition to already detected five series), the $^7\Sigma$ electronic state is preffered as the low lying Σ electronic state.

3-3-4-3. A New Metal Source to the Gas Phase

The author used the stainless steel hollow cathode discharge in a mixture of Ar and H_2S to produce FeS. The iron atom was supplied to the gas phase from the stainless steel hollow cathode by the sputtering of the stainless steel by Ar. Similar phenomena were also observed when the spectral lines of FeO and AlO were also produced in the cell by discharging a mixture of Ar and O_2 by using the stainless steel hollow cathode and an aluminum one, respectively. This method is a stable source of metals to the gas phase and easily applicable to production of heavy metal containing molecules with the conventional free space cell. In optical spectroscopy, hollow cathodes have been employed as a metal source as mentioned in Chapter 2, but this method may be widely applicable also to microwave spectroscopy.

3-3-4-4. Search for FeS in Space

The spectral lines in J=7-6 and 8-7 transitions of the $^5\Delta_4$ substate, which is the substate with lowest energy, were searched for toward IRC+10216, Orion-KL, Sgr B2, and W51. However, lines corresponding to FeS were not detected. The details will be described in Chapter 4.

REFERENCES

Brown, J.M., Cheung, A.S-C., and Merer, A.J. 1987, J. Molec. Spectrosc., **124**, 464.

Cernicharo, J., and Guélin, M. 1987, Astron. Astrophys., **183**, L10.

Cheung, A. S-C., Gordon, R.M., and Merer, A.J. 1981, J. Molec. Spectrosc., **87**, 289.

Engelking, P.C., and Lineberger, W.C. 1977, J. Chem. Phys., **66**, 5054.

Kröckertskothen, T., Knöckel, H., and Tiemann, E. 1986, Chem. Phys., **103**, 335.

Merer, A.J., Walmsley, C.M., and Churchwell, E. 1982, Astrophys. J., **256**, 151.

Narasimham, N.A., and Balasubramanian, T.K. 1971, J. Molec. Spectrosc., **37**, 371.

Taylor, A.W., Cheung, A. S-C., and Merer, A.J. 1985, J. Molec. Spectrosc., **113**, 487.

Tsuji, T. 1973, Astron. Astrophys., **23**, 441.

Verma, R.D., and Singhal, S.R. 1975, Can. J. Phys., **53**, 411.

Yamamoto, S., and Saito, S. 1988, J. Chem. Phys., **89**, 1936.

TABLE 1
Observed and calculated transition frequencies of the FeS radical ($^5\Delta_i$).

J'	-	J	Ω	Parity	$\nu_{obs.}$ (MHz)	$\nu_{obs.} - \nu_{calc.}$ (MHz)
v=0						
19	-	18	4		230383.569(17)[a]	-0.004
20	-	19	4		242497.470(26)	0.000
21	-	20	4		254609.589(7)	-0.001
22	-	21	4		266719.857(22)	0.015
23	-	22	4		278828.119(7)	-0.020
24	-	23	4		290934.432(15)	0.043
25	-	24	4		303038.498(14)	-0.008
26	-	25	4		315140.389(7)	-0.009
27	-	26	4		327239.984(13)	0.006
28	-	27	4		339337.110(15)	-0.046
29	-	28	4		351431.877(28)	0.035
30	-	29	4		363523.901(29)	-0.047
31	-	30	4		375613.419(14)	0.035
32	-	31	4		387700.062(19)	0.002
19	-	18	3		230980.325(21)	-0.046
20	-	19	3		243125.506(23)	0.013
21	-	20	3		255268.847(20)	0.040
22	-	21	3		267410.235(10)	0.010
23	-	22	3		279549.608(16)	-0.046
24	-	23	3		291687.058(26)	0.052
25	-	24	3		303822.226(31)	0.037
26	-	25	3		315955.100(11)	-0.013
27	-	26	3		328085.671(6)	-0.016
28	-	27	3		340213.814(7)	-0.006
29	-	28	3		352339.416(41)	-0.007
30	-	29	3		364462.341(41)	-0.063
31	-	30	3		376582.644(7)	-0.028
32	-	31	3		388700.210(12)	0.072
18	-	17	2		219664.503(61)	130.011[b]
			2		219666.863(47)	135.199
19	-	18	2		231859.268(55)	139.100
			2		231862.157(29)	145.306
20	-	19	2		244052.544(21)	148.435
			2		244056.082(17)	155.829
21	-	20	2		256244.535(21)	158.311
			2		256248.678(42)	166.903
22	-	21	2		268434.889(19)	168.467
			2		268439.870(37)	178.547
23	-	22	2		280623.677(35)	179.068
			2		280629.571(29)	190.767
24	-	23	2		292810.836(19)	190.142
			2		292817.794(41)	203.671

(continued)

25	-	24	2		304996.254(17)	201.668
			2		305004.388(23)	217.200
26	-	25	2		317179.928(22)	213.736
27	-	26	2		329361.779(22)	226.359
28	-	27	2		341541.789(50)	239.612
			2		341554.688(35)	262.774
29	-	28	2		353719.841(26)	253.470
			2		353734.839(23)	279.818
30	-	29	2		365895.983(19)	268.072
			2		365913.371(25)	297.967
31	-	30	2		378070.080(22)	283.377
			2		378090.227(25)	317.257
32	-	31	2		390242.182(10)	299.528
			2		390265.469(41)	337.844
Series(?) indicated by asterisks in Figure 1						
28	-	27	?		341979.634(19)	
29	-	28	?		354150.686(32)	
30	-	29	?		366335.364(19)	
31	-	30	?		378535.333(20)	
28	-	27	1	e	(342625.6)[c]	0.082
				f	(342719.2)	-0.148
29	-	28	1	e	(354834.7)	-0.047
				f	(354933.6)	0.239
30	-	29	1	e	(367041.0)	-0.097
				f	(367144.6)	-0.035
31	-	30	1	e	(379244.5)	0.030
				f	(379353.0)	-0.074
32	-	31	1	e	(391444.8)	0.033
				f	(391558.6)	0.017
Series indicated by squares in Figure 1						
28	-	27	0?		(343867.9)	
29	-	28	0?		(356123.5)	
30	-	29	0?		(368376.7)	
31	-	30	0?		(380627.2)	
32	-	31	0?		(392874.9)	

(continued)

v=1					
27	-	26	4	(325712.7)	-0.121[d]
28	-	27	4	(337753.3)	-0.102[d]
29	-	28	4	349791.530(30)	0.040
30	-	29	4	361826.971(5)	-0.025
31	-	30	4	373859.856(14)	0.027
32	-	31	4	(385889.7)	-0.201[d]
27	-	26	3	(326562.5)	-0.206[d]
28	-	27	3	338634.390(26)	0.019
29	-	28	3	350703.523(14)	0.023
30	-	29	3	362769.976(9)	-0.025
31	-	30	3	374833.785(34)	-0.001
32	-	31	3	(386894.8)	0.038

[a] One standard deviation of the frequency measurement in kHz.
[b] Weight is 0.0.
[c] The roughly measured frequency.
[d] Weight is 0.1.

TABLE 2
Observed transition frequencies of the FeS radical (low lying Σ state).

N'	-	N	$\nu_{obs.}$ (MHz)
Series 1			
23	-	22	(277527)[a]
24	-	23	
25	-	24	
26	-	25	
27	-	26	
28	-	27	(342916.4)
29	-	28	(355859.4)
30	-	29	(368757.9)
31	-	30	381613.707(45)[b]
32	-	31	(394428.2)
Series 2			
24	-	23	(295881.5)
25	-	24	
26	-	25	(321089.7)
27	-	26	(333671.2)
28	-	27	346238.598(16)
29	-	28	358792.332(8)
30	-	29	371333.321(13)
31	-	30	(383861.6)
32	-	31	
Series 3			
24	-	23	(298281.1)
25	-	24	
26	-	25	(323004.3)
27	-	26	(335369.7)
28	-	27	347736.898(34)
29	-	28	360105.104(35)
30	-	29	372473.982(11)
31	-	30	(384843.09)
32	-	31	
Series 4			
24	-	23	(301097.8)
25	-	24	
26	-	25	(325628.1)
27	-	26	(337905.6)
28	-	27	350189.880(22)
29	-	28	362480.421(9)
30	-	29	374776.380(18)
31	-	30	(387076.9)

(continued)

Series 5			
17	-	16	223176.888(3)
18	-	17	234912.782(12)
19	-	18	246649.625(8)
20	-	19	258396.986(23)
21	-	20	270162.747(22)
22	-	21	281953.151(24)
23	-	22	293772.992(6)
24	-	23	305625.384(4)
25	-	24	317512.039(23)
26	-	25	329433.684(44)
27	-	26	341389.943(79) disturbed
28	-	27	353379.604(24)
29	-	28	365401.285(16)
30	-	29	377452.879(16)
31	-	30	389532.251(14)

[a] The roughly measured frequency.
[b] One standard deviation of the frequency measurement in kHz.

TABLE 3
The molecular constants of FeS in the $^5\Delta_i$ electronic state (in MHz).

Constants	v=0 (Ω=4,3,1)	v=1 (Ω=4,3)
A_{SO}	−1339974(5732) [a]	−3000000[b]
B	6106.1575(20)	6063.9520(33)
D	0.00395287(66)	0.0038102(19)
λ	−47058(955)	—
λ_D	−0.2318(15)	−0.662237(87)
A_D	2.381(62)	—
$\tilde{n}_\Delta$	10.733(55)	—
$\tilde{o}_\Delta$	1.053(10)	—

[a] The values in parentheses are one standard deviations and apply to the last digits of the constants.
[b] Fixed.

TABLE 4
The effective rotatioal constants and centrifugal distortion constants for each substate in the $^5\Delta_i$ electronic state of FeS (in MHz).

Ω	B_{eff}	D_{eff}	S.D.[a]
4	6065.40069(55) [b]	0.00370458(36)	0.028
3	6081.15074(52)	0.00376545(35)	0.021
2[c]	6103.7869	0.0030921	0.5 [d]
1e	6124.8088(46)	0.0041426(25)	0.056
1f	6126.1369(30)	0.0039228(16)	0.034
1[c]	6125.4779(58)	0.0040352(32)	0.072
0?	6146.4632(91)	0.0038057(50)	0.113

[a] One standard deviation of the fit.
[b] The values in parentheses are one standard deviations and apply to the last digits of the constants.
[c] The average frequency was used.
[d] The systematic residuals remain.

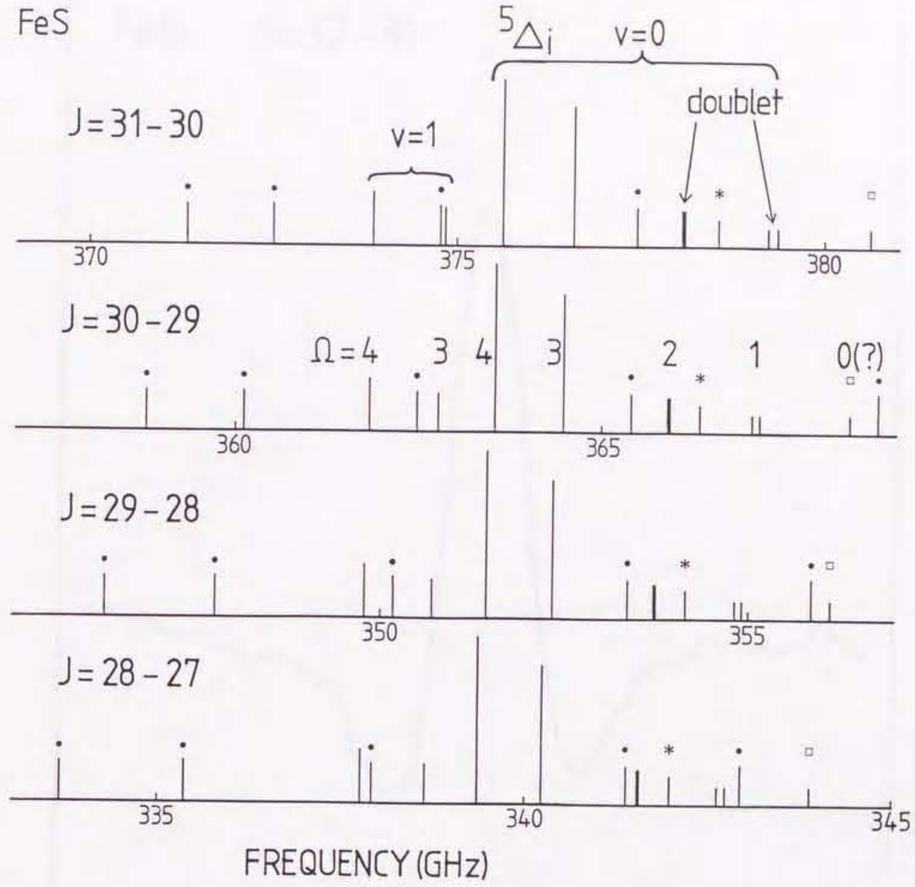

Figure 1: The spectral lines of FeS are shown schematically. The frequency axis is indicated at the intervals of 12 GHz. The ordinate corresponds to the relative intensity. The lines indicated by "●" show larger Zeeman effect and belong to a low lying Σ electronic state. The lines indicated by "∗" have not been considered to form a series (see the text). The assignment of the lines indicated by "□" is not yet clear (see the text).

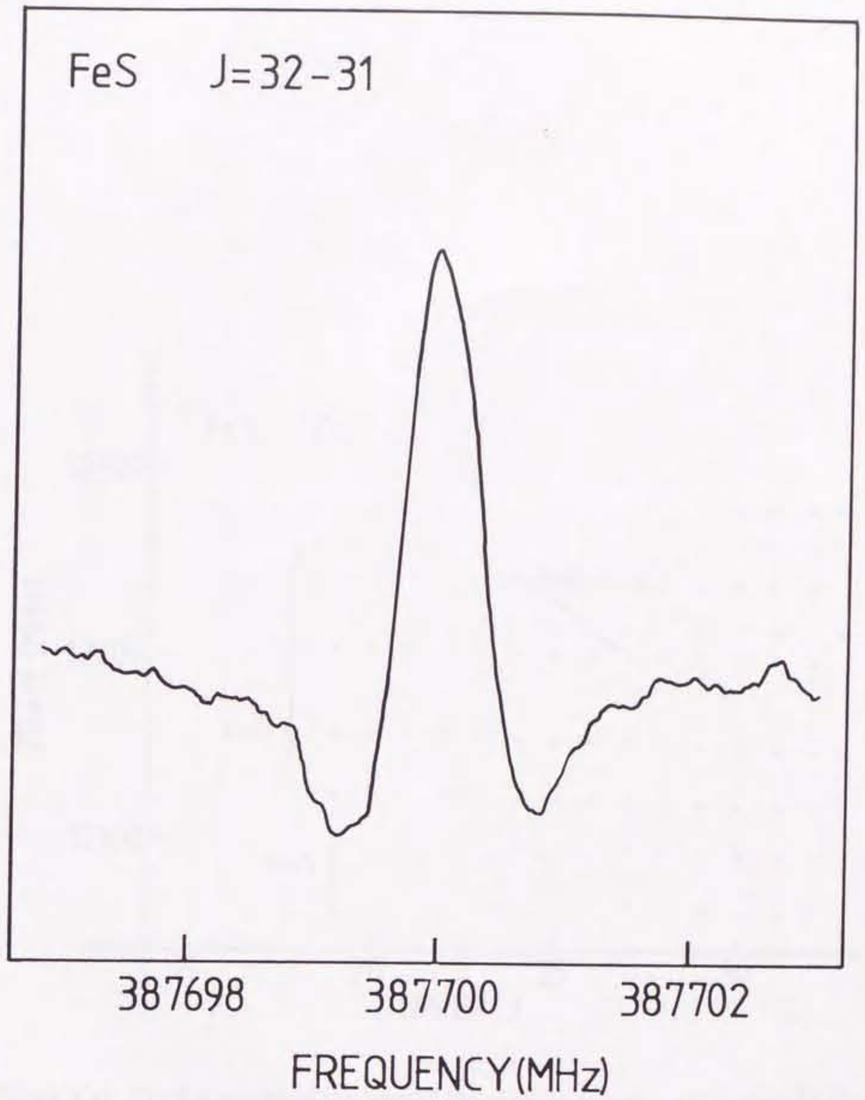

Figure 2: The J=32-31 rotational spectral line of FeS in the $^5\Delta_4$ substate at 387.7 GHz. The integration time is about 12 seconds with PSD time constant of 1 ms.

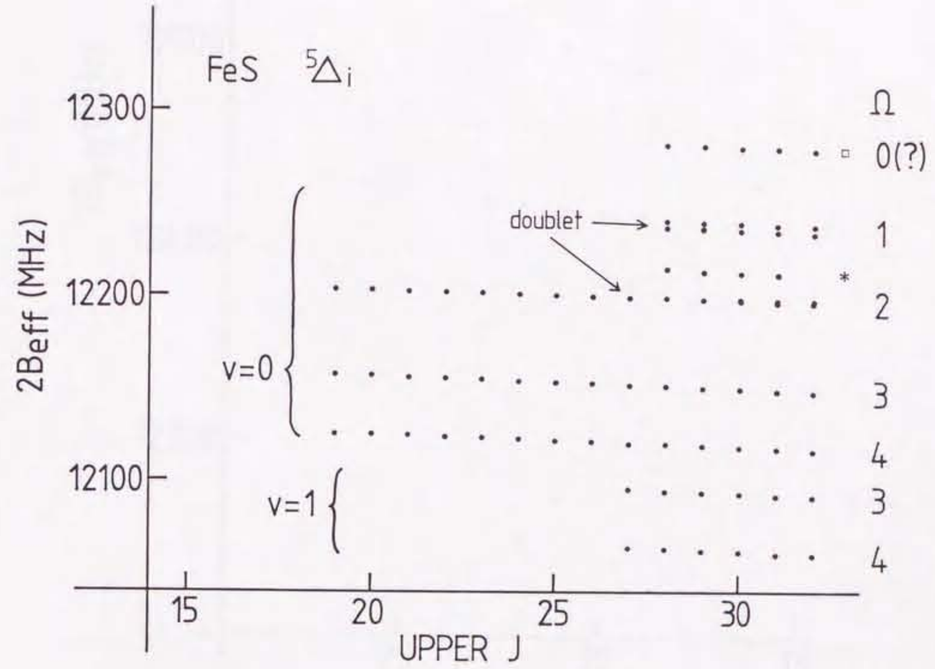

Figure 3(a): The frequencies of the lines of the series in Figure 1 are divided by the rotational quantum number, and the resulted $2B_{eff}$ values are plotted versus the rotational quantum numbers of the upper levels. The result of the series with linear $2B_{eff}$ behavior against the rotational quantum number is shown. The series indicated by "$*$"and "$\square$" are the same series indicated by same marks in Figure 1.

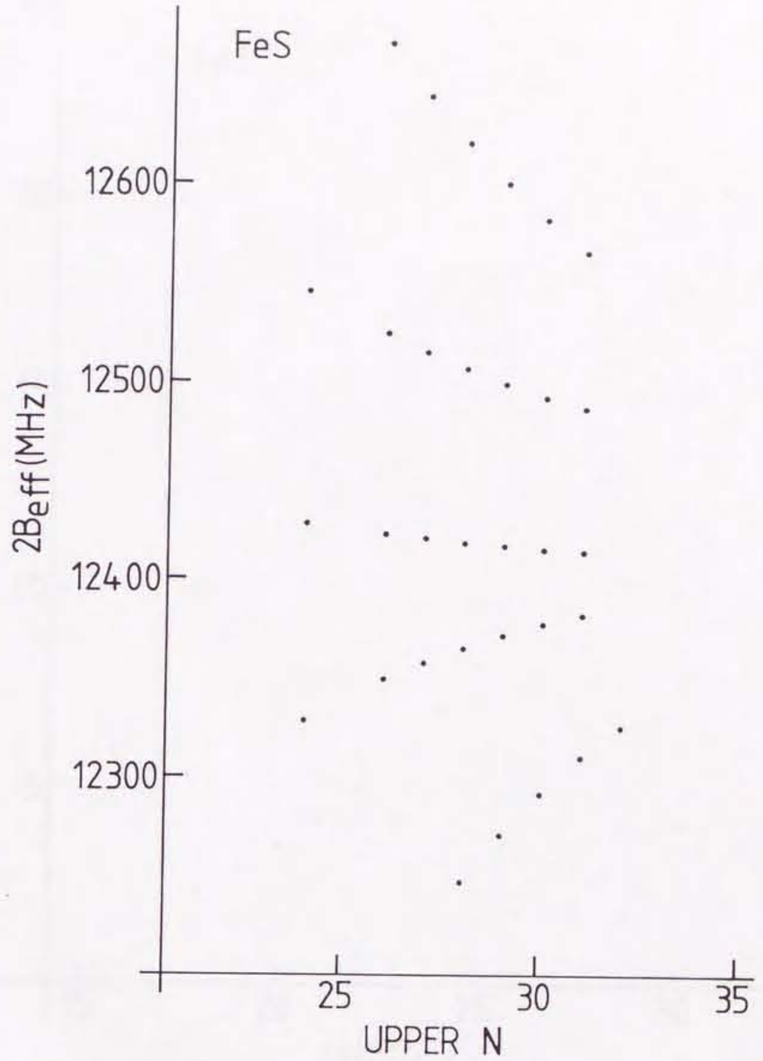

Figure 3(b): The result of the series with non-linear $2B_{eff}$ behavior against the rotational quantum number is shown. Only the five series indicated by closed circles in Figure 1 belong to these groups.

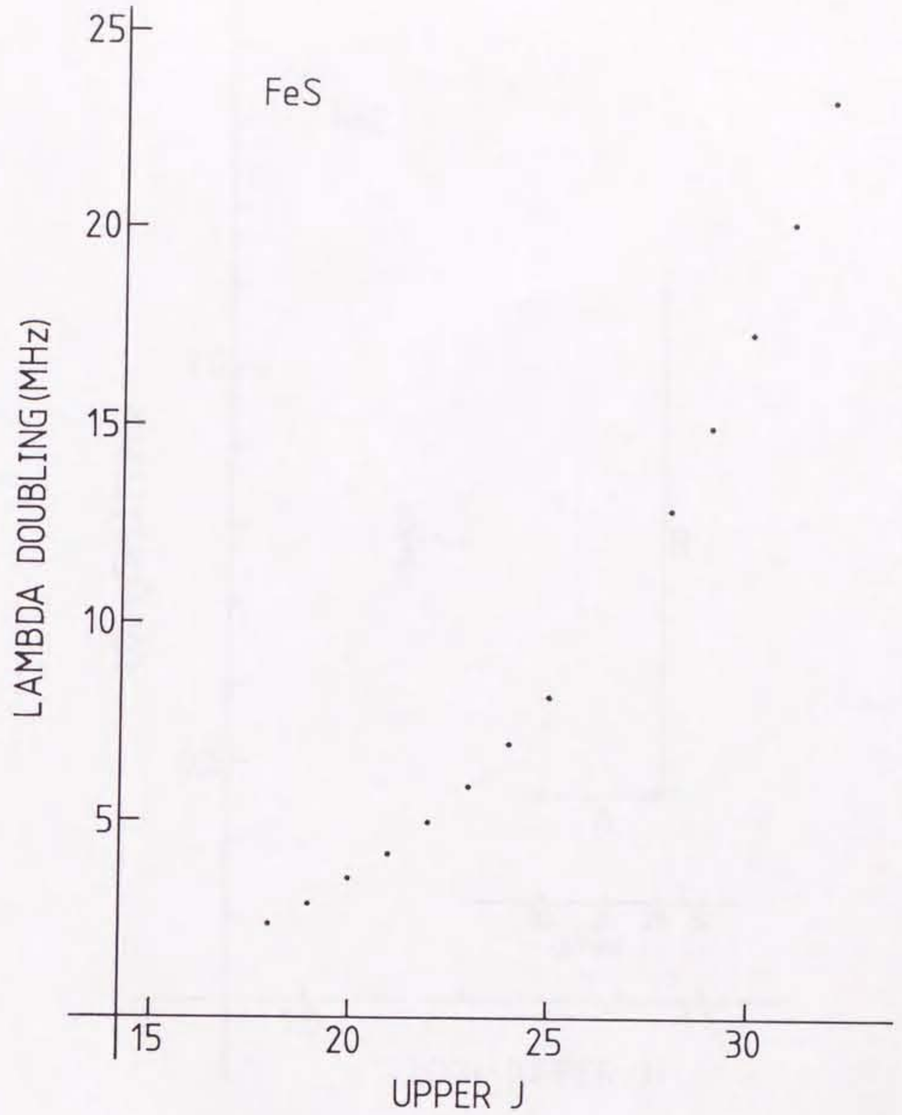

Figure 4(a): The frequency separations of the Λ-doubling in the $^5\Delta_2$ substate are plotted against the rotational quantum number.

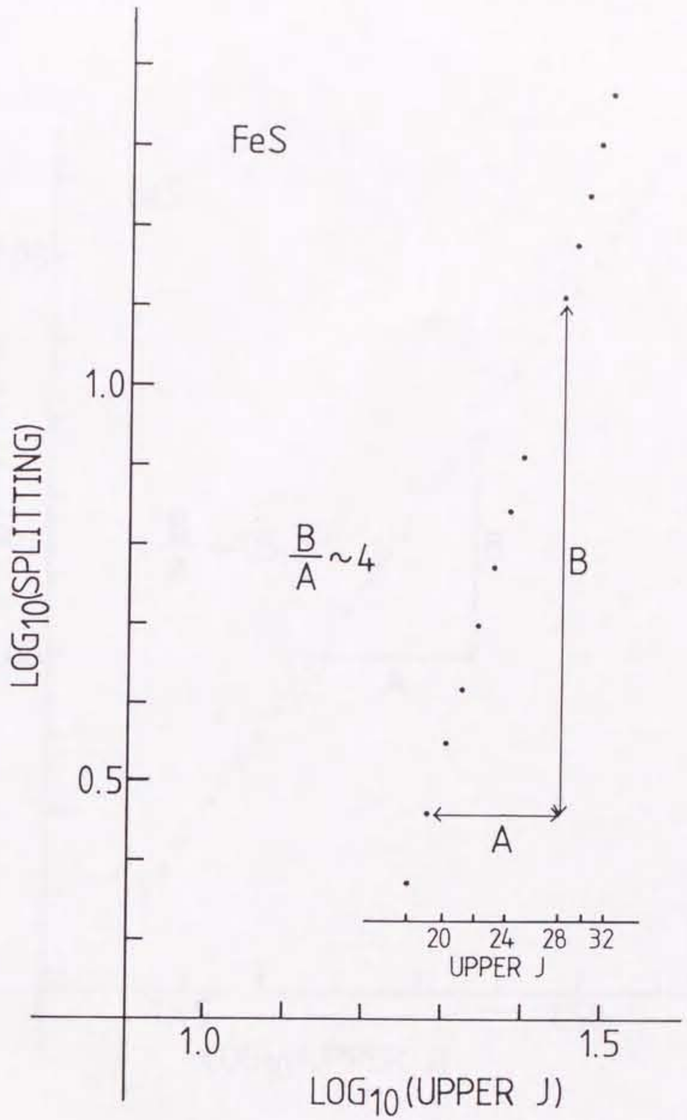

Figure 4(b): Same as (a), but the scale in both axes is in logarithm. The separations were found to be proportional to roughly J^4.

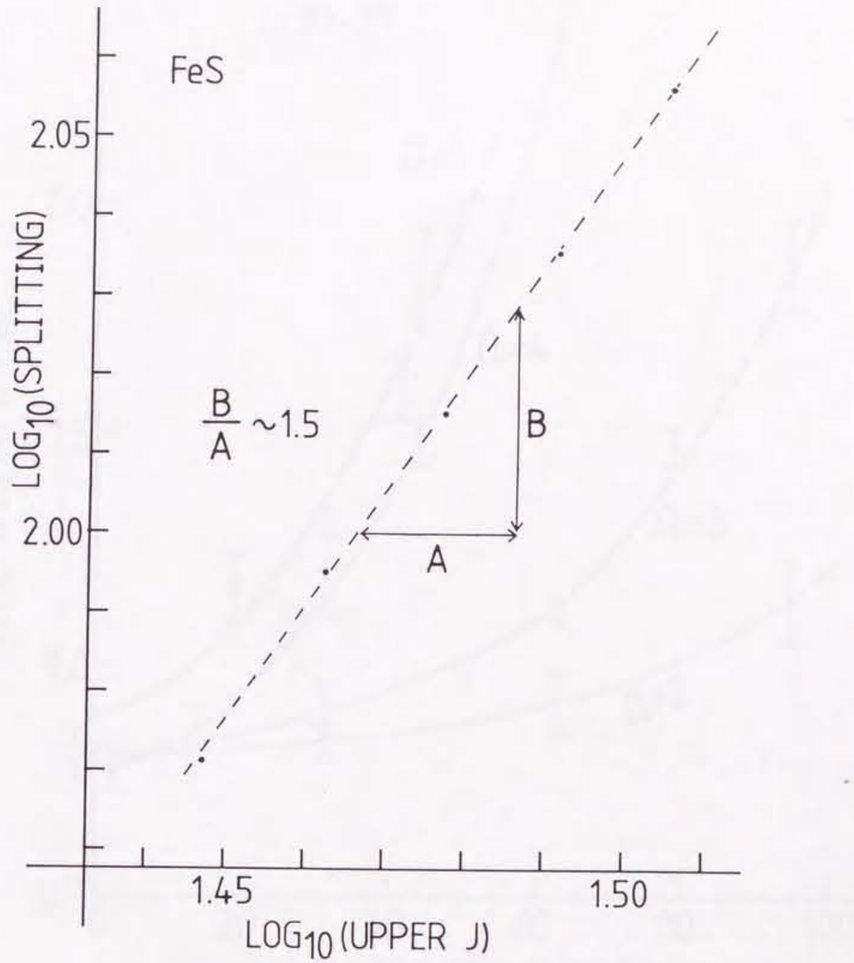

Figure 5: The frequency separations of the Λ-doubling in the $^5\Delta_1$ substate are plotted against the rotational quantum number. The scale in both axes is in logarithm. The separations were found to be proportional to roughly $J^{1.5}$.

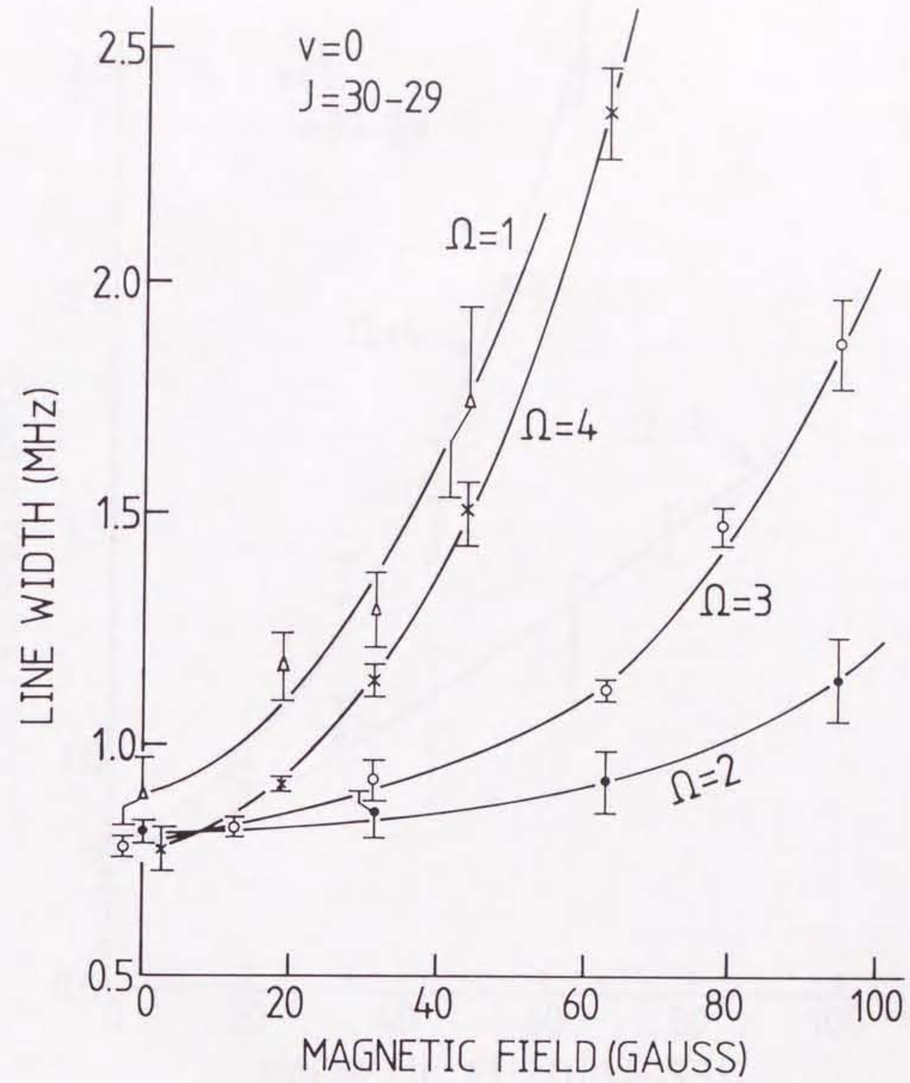

Figure 6(a): The Zeeman effect of each substate in the $^5\Delta_i$ electronic state in the v=0 vibrational state.

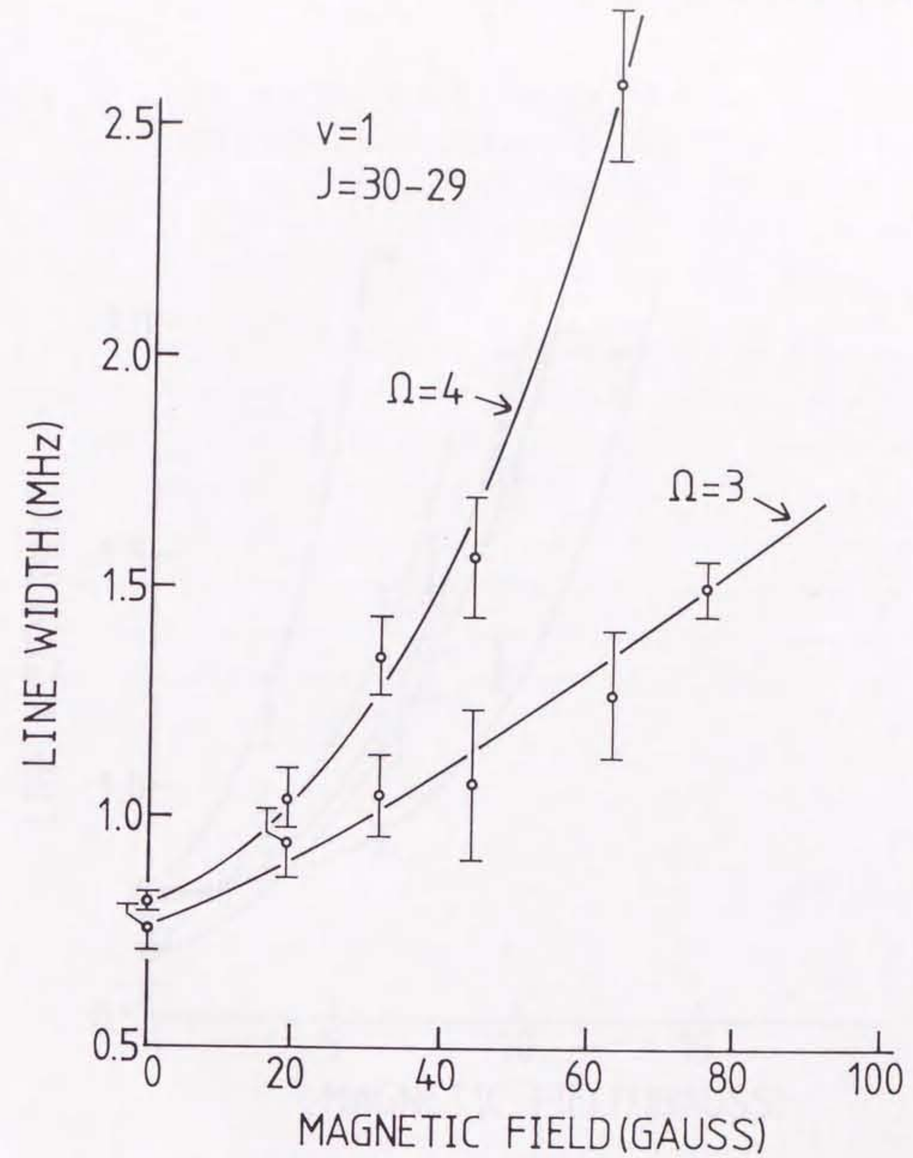

Figure 6(b): The Zeeman effect of each substate in the $^5\Delta_i$ electronic state in the v=1 vibrational state.

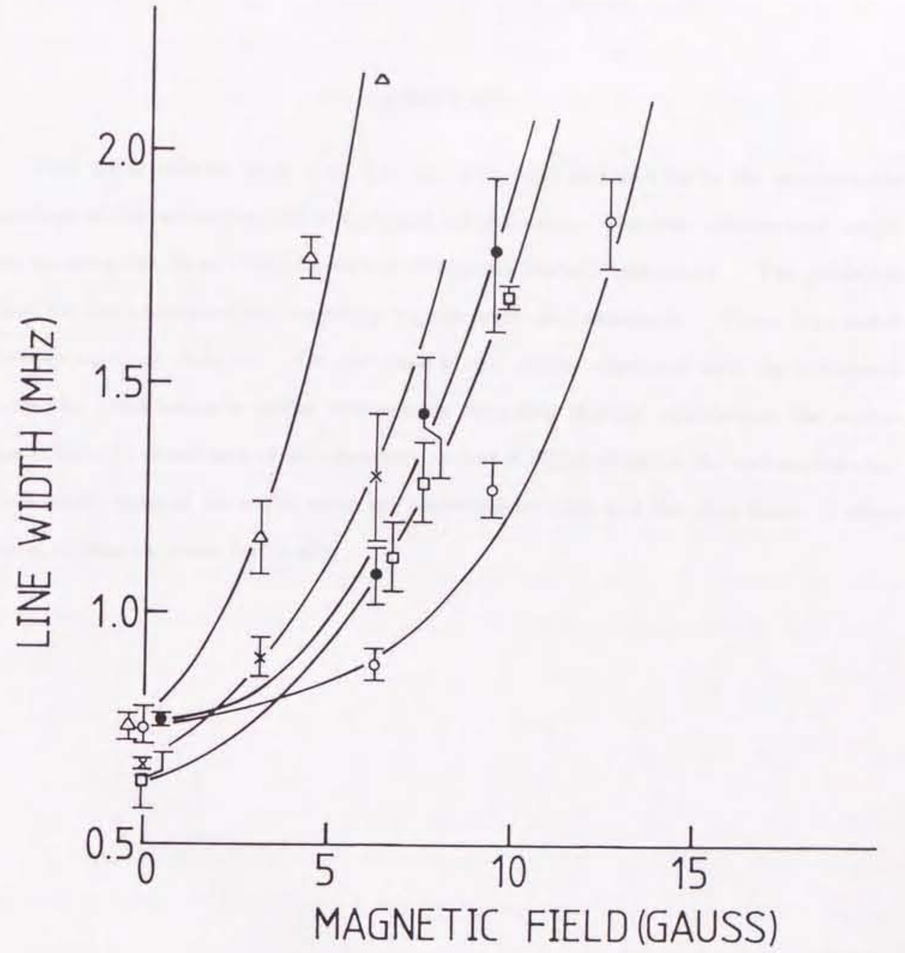

Figure 7: The Zeeman effect of each substate in the low lying Σ electronic state; " ○ " Series 5 J=29-28, " □ " Series 2 J=29-28, " ● " Series 4 J=29-28, " × " Series 3 J=29-28, " △ " Series 1 J=30-29.

Chapter 4. Searches for the Metal Sulfides in the Circumstellar Envelope of IRC+10216

ABSTRACT

Four metal sulfides, MgS, CaS, AlS, and FeS, were searched for in the circumstellar envelope of the carbon star IRC+10216 and other sources. The observations were carried out by using the 45 m radiotelescope at Nobeyama Radio Observatory. The published data for the corresponding frequency regions were also examined. These four metal sulfides were not detected. On the basis of our results combined with the calculated molecular abundances in stellar atmospheres assuming thermal equilibrium, the author found that the abundance of SiO decreases as that of SiS increases in the carbon-rich star. As a result, most of the sulfur atom are converted into SiS and the abundances of other metal sulfides decrease drastically.

4-1. Introduction

As described in Chapter 1, the metal sulfides were predicted to be relatively abundant in cool stellar atmospheres by a thermal equilibrium calculation (Tsuji 1973). Based on the results of the laboratory millimeter-wave spectroscopy of MgS, CaS, AlS, and FeS, which were already described in Chapter 3, these molecules were searched for in the circumstellar envelope of the carbon star IRC+10216 and other sources with radiotelescopes.

The envelope of IRC+10216 is known by rich molecular lines. This may be due to active molecular formation and also due to the relatively short distance (200 pc) from the earth as explained in Chapter 1. Various molecules have been detected in this envelope. In particular, molecules containing refractory elements, Na, K, Al, Si, and P, have been found in this envelope: SiO, SiS (Morris 1975), SiC_2 (Thaddeus, Cummins, and Linke 1984), SiH_4 (Goldhaber and Betz 1984), NaCl, AlCl, KCl, and AlF (Cernicharo and Guélin 1987a), SiC (Cernicharo et al. 1989), SiC_4 (Ohishi et al. 1989), and CP (Guélin et al. 1990). Therefore, this envelope seems to be the most suitable source to search for the metal sulfides.

4-2. Observations

The observations were carried out by using the 45 m radiotelescope at Nobeyama Radio Observatory (NRO) in 1989 April, 1990 March, and 1990 May for MgS, AlS, and FeS, respectively. The observed source parameters and the details of the observations are summarized in Table 1 and 2, respectively. The observed sources other than IRC+10216 are warm sources, Orion-KL (massive star forming region), Sgr B2 (our galactic center), W51A (massive star forming region), and DR21(OH) (low mass star forming region), because active and hot circumstances must be necessary to vaporization of metals. The metal sulfides were searched for in 80-100 GHz region. The beam size is also listed in

Table 2. A cooled Schottky diode mixer receiver (M100) and an SIS mixer receiver (S100) were used. The system temperatures were between 600 and 1000 K for the MgS search, 450 K for the AlS search, and between 600 and 800 K for the FeS search including the atmospheric attenuation. Acousto-optical radio spectrometers were used as the backend. The frequency resolution of the spectrometer is 250 kHz with the bandwidth of 250 MHz. The pointing was checked every two hours by observing a nearby SiO maser source, R-Leo, for IRC+10216. The accuracy of the pointing was better than 5" in ordinary condition. The position-switching mode was used. The antenna temperature was calibrated by the usual chopper-wheel method.

4-3. Results

The spectral line features of MgS, CaS, AlS, and FeS were not detected at their corresponding transition frequencies. The upper limits to the column densities were calculated assuming local thermal equilibrium of the optically thin line and the results are listed in Table 2 and 3. The dipole moment assumed was 2.0 Debye for MgS, CaS, and AlS, because no experimental determinations and theoretical predictions were reported. The dipole moment of FeS was assumed to be the same as that of FeO (4.7 Debye, Steimle et al. 1989). The rotational temperature and the line width assumed were listed in Table 1. The observed spectra of IRC+10216 at the transition frequencies of MgS (J=6-5), AlS (J=6-5), and FeS (J=8-7) were shown in Figure 1, 2, and 3, respectively. CaS was examined only in the published data of the corresponding frequency region toward IRC+10216 (J=7-6, Figure 1a in Cernicharo et al. 1986 or Figure 1 in Cernicharo et al. 1987b; J=8-7, Figure 1c in Guélin et al. 1987a). The results are listed in Table 3 and the spectra are shown in Figure 4. AlS was also examined in the published data of the corresponding frequency region toward Sgr B2 (N=6-5; Figure 1b in Cernicharo et al. 1988), and toward IRC+10216 (N=8-7; Figure 1 in Guélin et al. 1987b). The results are listed in Table 3 and the spectra are shown in Figure 5.

The source sizes were assumed to be 15" for IRC+10216, and the effect of the beam dilution was taken into account in the calculation of the upper limits. For other sources, the sources were assumed to fill the main beam.

4-4. Discussion of the Upper Limits to the Column Density

The upper limits to the column density of the metal sulfides in IRC+10216 are collected in Table 4. In this Table, the column density of the one of the most abundant sulfide SiS and other molecules containing refractory elements are also listed. The upper limits of MgS, CaS, and FeS are $10^{12} \sim 10^{13}$ cm^{-2}, but that of AlS is much larger (1x10^{14} cm^{-2}). The reason is that the fine and hyperfine components of AlS increased the partition function by about one order. The upper limits of the metal sulfides are two or three orders of magnitude lower than the column density of SiS. This may originate from the stability of the Si–S bond, which is expected from the bond energies (see Table 4). In addition, other reasons may decrease the abundances of the metal sulfides. (1) The unknown stable molecules containing Mg, Ca, Al, or Fe may be the major species of the metal containing compounds, so that free metals available for the metal sulfides decrease. In the case of Al, the two halides, AlCl and AlF have column densities 2x10^{14} (3x10^{-9}) and 4x10^{13} cm^{-2} (7x10^{-10}), respectively (Table 4) (Guélin and Cernicharo 1988). The values in parentheses indicate the fractional abundances relative to H_2. The H_2 column density adopted was 6x10^{22} cm^{-2} (Keady and Hinkle 1988). Since the cosmic abundance of aluminum relative to H_2 is 5x10^{-6}, the column densities of AlCl and AlF are not large enough to explain the abundance of Al in the envelope. (2) The depletion of metals from the gas phase to the dust grain may be important.

The further quantitative discussion must be based on the thermal equilibrium calculation of the stellar atmosphere in a carbon-rich condition if most of these metal sulfides are produced by the reaction in thermal equilibrium condition. Recently, the molecular abundances in stellar atmospheres in the carbon-rich condition was calculated by Tsuji

(1990). The calculations were carried out including about 600 molecules. The total pressure of the gas was assumed to be 10^3 dyn cm^{-2} and the C/O ratio was assumed to be 2.0. If the C/O ratio is changed, the abundances of oxides and carbides are affected, but those of other molecules hardly affected. There is no observational information on the total pressure, which was assumed to be 10^3 dyn cm^{-2}, the same pressure used in Figures $2 \sim 5$ in Chapter 1. On the other hand, McCabe, Smith, and Clegg (1979) reported that 100 dyn cm^{-2} was appropriate based on their thermal equilibrium model. The results for the metal sulfides, metal oxides, and related molecules containing refractory elements were shown in Figure 6. According to the calculation, SiS and SiO are the most abundant molecules (fractional abundances $10^{-4.5} \sim 10^{-5}$ at $900 \sim 1600$ K). The observed abundances of SiS and SiO are low by about two orders of magnitude at about 1600 K, which is proposed as the photospheric temperature of IRC+10216 (Lafont, Lucas, and Omont 1982). This low abundance may indicate depletion. The abundance of AlF and AlCl are relatively larger ($10^{-6} \sim 10^{-8}$) than those of NaCl and KCl ($10^{-7.5} \sim 10^{-10}$). For these metal halides, the observed abundances are lower by about one order of magnitude than the calculated abundances at about 1600 K. The metal sulfides are $3 \sim 4$ orders of magnitude less abundant ($10^{-11} \sim 10^{-14}$) than NaCl or KCl. The metal oxides are much less abundant than the metal sulfides by $2 \sim 3$ orders of magnitude ($10^{-15} \sim 10^{-17}$). Therefore, it is clear that the metal sulfides are relatively more abundant than the metal oxides as already discussed in Chapter 1. The calculated fractional abundance of the metal sulfides (MgS, CaS, AlS, and FeS) is consistent with their non-detections in IRC+10216, because their upper limits of the fractional abundance are $10^{-9} \sim 10^{-11}$ while the calculated fractional abundances are about 10^{-13} at 1600 K.

The calculated low fractional abundances are considered to be due to the low abundance of free sulfur available for the metal sulfides. This is because the abundance of SiO decreaces as the C/O ratio increases in the carbon star, that is, the abundance of SiS increases. As a result, most of the sulfur atoms are converted into SiS and the abun-

dances of other metal sulfides decrease heavily. The fractional abundance of SiS is about $10^{-4.5}$ whereas the cosmic fractional abundance of sulfur is also about $10^{-4.5}$ (Table 2 in Chapter 1).

In the envelope of oxygen-rich stars, SiS cannot lock up most of sulfur. Silicon reacts with the excess oxygen to form SiO which is stabler than SiS (see the bond energies in Table 4). As a result, the fractional abundance of SiS in the oxygen-rich envelope (about $10^{-5.5}$ at 1600 K; Figure 7) is lower than that in the carbon-rich envelope (about $10^{-4.5}$ at 1600 K; Figure 6), and the fractional abundances of the metal sulfides in the oxygen-rich envelope (about 10^{-9} at 1600 K; Figure 2 $\sim$ 5 in Chapter 1) are relatively higher than those in the carbon-rich envelope (about 10^{-13} at 1600 K; Figure 6). Therefore, there still remains a possibility to detect the metal sulfides in oxygen-rich envelopes.

It has been known that the abundances of some molecules containing refractory elements cannot be explained only by thermal equilibrium model. In the case of CP, the abundance in IRC+10216 is higher than that predicted by the thermal equilibrium calculation (Guélin et al. 1990). In the case of SiC (Cernicharo et al. 1989), its distribution in the envelope of IRC+10216 extends to at least 54" in diameter. This distribution is unexpectedly larger for such nonvolatile compound. Therefore, SiC is considered to be produced by the photodissociation of SiC_2 by the interstellar radiation. However, in the case of four metal sulfides, there seems to be no efficient production mechanism except thermal equilibrium reaction.

As a result, the author made clear the behavior of the sulfur atom in the molecules found in the circumtellar envelope of the carbon star. In future, more extensive interstellar observations must be carried out, and more detailed model calculations, including the effect of the gradient of temperature and pressure, and the depletion of atoms and molecules forming dust grains, are needed to examine and understand the chemistry in the circumstellar envelope quantitatively.

REFERENCES

Baars, J.W.M, Hooghoudt, B.G., Mezger, P.G., and de Jonge, M.J. 1987,
Astron. Astrophys., **175**, 319.

Cernicharo, J., Gottlieb, C.A., Guélin, M., Thaddeus, P., and Vrtilek, J.M. 1989,
Astrophys. J., **341**, L25.

Cernicharo, J., and Guélin, M. 1987a, Astron. Astrophys., **183**, L10.

Cernicharo, J., Guélin, M., Hein, H., and Kahane, C. 1987c,
Astron. Astrophys., **181**, L9.

Cernicharo, J., and Guélin, M., Menten, K.M., and Walmsley, C.M. 1987b,
Astron. Astrophys., **181**, L1.

Cernicharo, J., Kahane, C., Gomez-Gonzalez, J., and Guélin, M. 1986,
Astron. Astrophys., **164**, L1.

Cernicharo, J., Kahane, C., Guélin, M., and Gomez-Gonzalez, J. 1988,
Astron. Astrophys., **189**, L1.

Goldhaber, D.M., and Betz, A.L. 1984, Astrophys. J., **279**, L55.

Guélin, M., and Cernicharo, J. 1988, 'The physics and chemistry of interstellar
molecular clouds' (Springer-Verlag, Lecture notes in physics,
Eds. Winnewisser, G., and Armstrong, J.T.)

Guélin, M., Cernicharo, J., Kahane, C., Gomez-Gonzalez, J., and Walmsley, C.M. 1987a,
Astron. Astrophys., **175**, L5.

Guélin, M., Cernicharo, J., Navarro, S., Woodward, D.R., Gottlieb, C.A., and
Thaddeus, P. 1987b, Astron. Astrophys., **182**, L37.

Guélin, M., Cernicharo, J., Paubert, G., and Turner, B.E. 1990,
Astron. Astrophys., **230**, L9.

Keady, J.J., and Hinkle, K.H. 1988, Astrophys. J., **331**, 539.

Lafont, S., Lucas, R., and Omont, A. 1982, Astron. Astrophys., **106**, 201.

Morris, M. 1975, Astrophys. J., **197**, 603.

Ohishi, M., Kaifu, N., Kawaguchi, K., Murakami, A., Saito, S.,
Yamamoto, S., Ishikawa, S., Fujita, Y., Shiratori, Y., and Irvine, W.M. 1989,
Astrophys. J., **345**, L83.

Ohishi, M., Yamamoto, S., Saito, S., Kawaguchi, K., Suzuki, H., Kaifu, N., Ishikawa, S.,
Takano, S., Tsuji, T., and Unno, W. 1988, Astrophys. J., **329**, 511.

Padin, S., Sargent, A.I., Mundy, L.G., Scoville, N.Z., Woody, D.P., Leighton, R.B.,
Masson, C.R., Scott, S.L., Seling T.V., Stapelfeldt, K.R.,
and Terebey, S. 1989, Astrophys. J., **337**, L45.

Saito, S., Yamamoto, S., Kawaguchi, K., Ohishi, M., Suzuki, H., Ishikawa, S.,
and Kaifu, N. 1989, Astrophys. J., **341**, 1114.

Steimle, T.C., Nachman, D.F., Shirley, J.E., and Merer, A.J. 1989,
J. Chem. Phys., **90**, 5360.

Thaddeus, P., Cummins, S., and Linke, R.A. 1984, Astrophys. J., **283**, L45.

Tsuji, T. 1973, Astron. Astrophys., **23**, 441.

Tsuji, T. 1990, private communication.

TABLE 1

Parameters of the observed sources

Source	α(1950.0)	δ(1950.0)	T_{ex}(K)	Δv (km s^{-1})
IRC+10216	$09^h45^m15.^s0$	13°30'45."0	17[a]	27[a]
Orion-KL	05 32 46.9	-05 24 23	100[b]	15[b]
Sgr B2	17 44 11.1	-28 22 30	50[b]	20[b]
W51A	19 21 26.2	14 24 43.6	50[c]	27[c]
DR21(OH)	20 37 13.9	42 12 00.0	50[d]	4.3[e]

[a] From NaCl (Cernicharo and Guélin 1987a).

[b] Ohishi et al. 1988.

[c] Saito et al. 1989.

[d] Padin et al. 1989.

[e] From the HC_3N J=11-10 spectral line observed simultaneously in DR21(OH).

TABLE 2

Summary of the observations

Molecule	Transition	Frequency (MHz)	Beam[a] (")	Source	rms[b] (mK)	RX	η_b [c]	Column Density (cm^{-2})
MgS	J=6-5	96075.985	17.5	IRC+10216	13	M100	0.45	$\leq 1 \times 10^{13}$
AlS ($^2\Sigma^+$)	J=6-5	100400.[d]	16.7	IRC+10216	19	S100	0.38	$\leq 1 \times 10^{14}$
				DR21(OH)	24	S100	0.38	$\leq 4 \times 10^{13}$
FeS ($^5\Delta_4$)	J=7-6	84910.47	19.8	IRC+10216	17	M100	0.5	$\leq 3 \times 10^{12}$
				Orion-KL	24	M100	0.5	$\leq 4 \times 10^{12}$
				Sgr B2	29	M100	0.5	$\leq 4 \times 10^{12}$
	J=8-7	97038.76	17.3	IRC+10216	11	S100	0.38	$\leq 3 \times 10^{12}$
				Orion-KL	15	S100	0.38	$\leq 3 \times 10^{12}$
				Sgr B2	19	S100	0.38	$\leq 3 \times 10^{12}$
				W51A	29	S100	0.38	$\leq 5 \times 10^{12}$

[a] The beam size (HPBW) of the NRO 45 m radiotelescope calculated by using a formula $16.''8/(freq[GHz]/100GHz)$.

[b] The rms noise in antenna temperature in emission free region.

[c] The main beam efficiency.

[d] The rotational transition consists of 12 fine and hyperfine components.

TABLE 3

Results from the already published data of the corresponding frequency region

Molecule	Transition	Frequency (MHz)	Beam[a] (")	Source	rms[b] (mK)	η_b [c]	Column density (cm^{-2})
CaS	J=7-6	73974.40	32.6	IRC+10216	10	0.65	$\leq 1x10^{13}$
	J=8-7	84540.68	28.6	IRC+10216	10	0.65	$\leq 1x10^{13}$
AlS	J=6-5	100400.[d]	24.1	Sgr B2	30	0.65	$\leq 1x10^{14}$
	J=8-7	133900.[d]	18.0	IRC+10216	20	0.65	$\leq 2x10^{14}$

[a] The beam size (HPBW) of the IRAM 30 m radiotelescope. The calculation of the beam size was carried out by the extrapolation of the actual value 21."0 at 2.6 mm (Baars et al. 1987).

[b] The estimated rms noise in antenna temperature in emission free region.

[c] The main beam efficiency of the IRAM 30 m radiotelescope. Estimated from Baars et al. 1987.

[d] The rotational transition consists of 12 fine and hyperfine components.

TABLE 4

The upper limits to the column density in IRC+10216

Molecule	Column Density (cm^{-2})	Fractional Abundance[a]	Bond Energy (kcal mol^{-1})
Sulfides			
MgS	$\leq 1x10^{13}$	$\leq 2x10^{-10}$	68
CaS	$\leq 1x10^{13}$	$\leq 2x10^{-10}$	74
AlS	$\leq 1x10^{14}$	$\leq 2x10^{-9}$	88
FeS	$\leq 3x10^{12}$	$\leq 5x10^{-11}$	76
SiS	$7x10^{15}$ [b]	$1x10^{-7}$	147
Other Molecules Containing Refractory Elements			
SiO	$2x10^{15}$ [c]	$3x10^{-8}$	190
NaCl	$5x10^{12}$ [c]	$8x10^{-11}$	97
AlF	$4x10^{13}$ [c]	$7x10^{-10}$	158
AlCl	$2x10^{14}$ [c]	$3x10^{-9}$	117
KCl	$2x10^{12}$ [c]	$3x10^{-11}$	101

[a] The H_2 column density adopted was $6x10^{22}$ cm^{-2} (Keady and Hinkle 1988).

[b] Cernicharo et al. 1987c.

[c] Guélin and Cernicharo 1988.

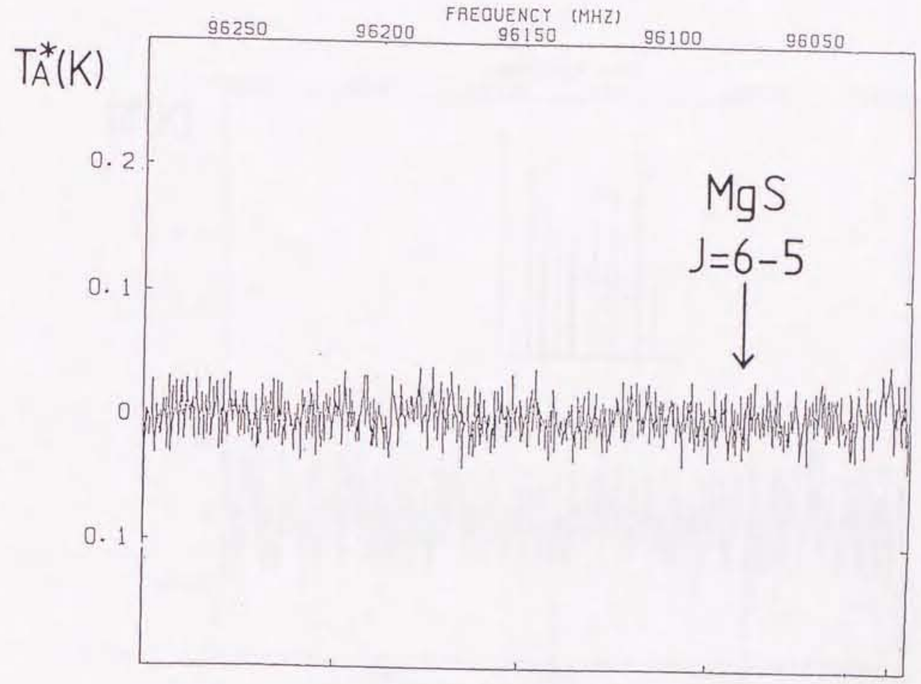

Figure 1: The obtained spectrum of the search for MgS toward IRC+10216.

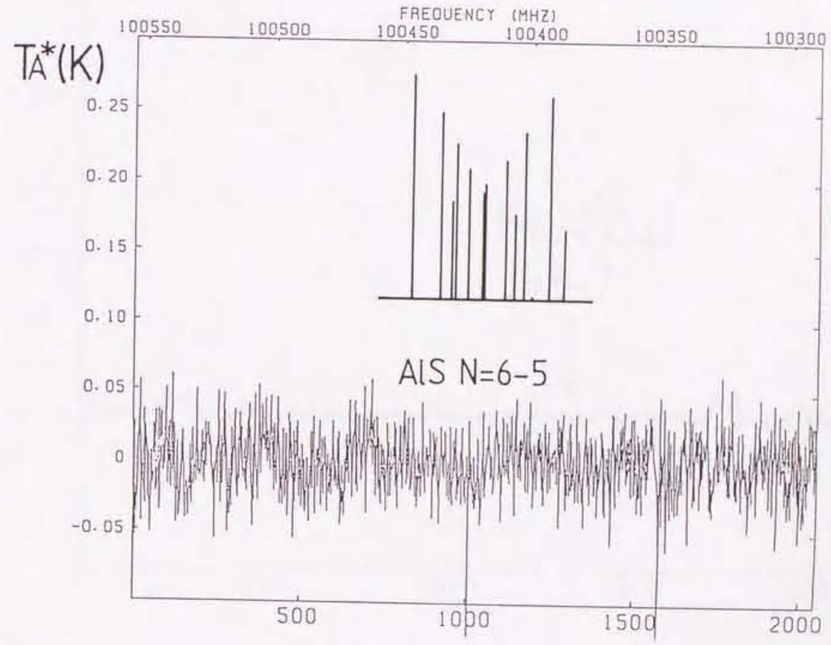

Figure 2: The obtained spectrum of the search for AlS ($^2\Sigma^+$) toward IRC+10216. The 12 fine and hyperfine components were indicated schematically.

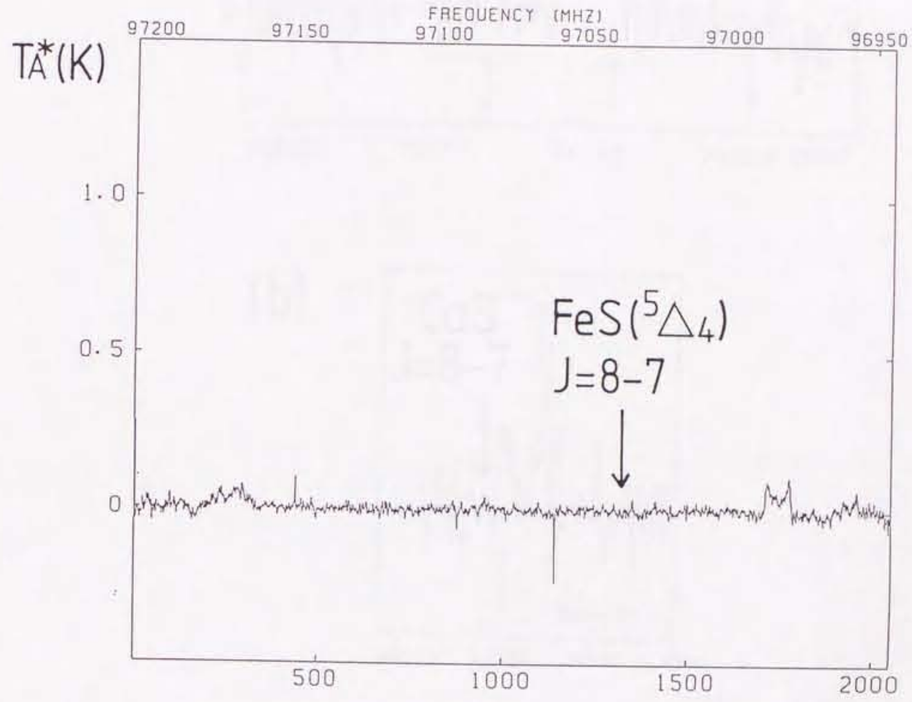

Figure 3: The obtained spectrum of the search for FeS ($^5\Delta_4$) toward IRC+10216.

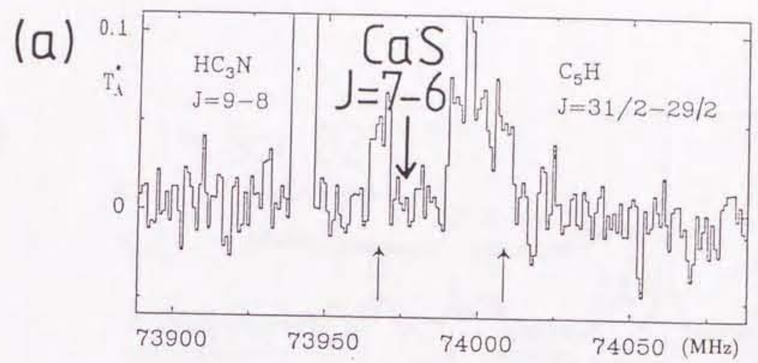

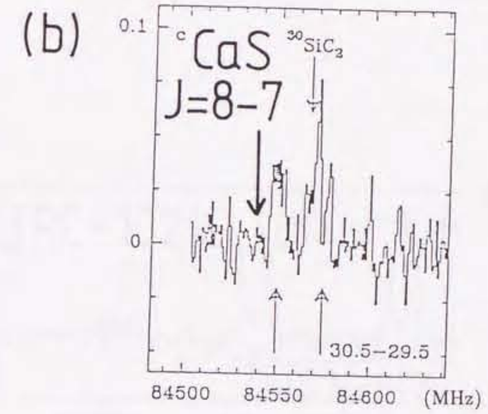

Figure 4: The already published spectra of the corresponding frequency region of the rotational transition of CaS toward IRC+10216. (a) J=7-6 (Cernicharo et al. 1987b), and (b) J=8-7 (Guélin et al. 1987a).

(a)

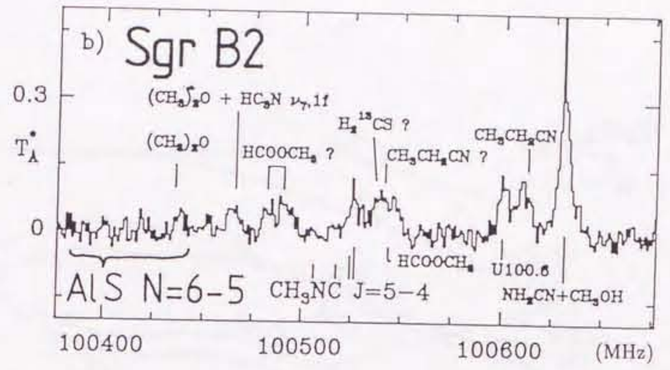

(b)

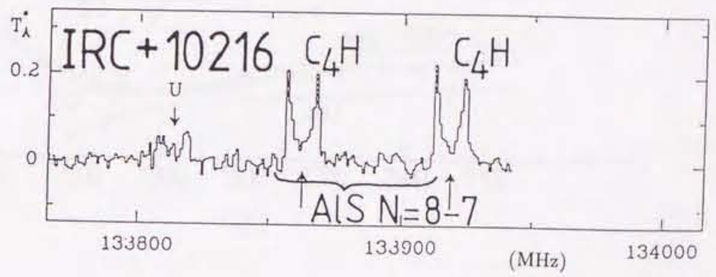

Figure 5: The already published spectra of the corresponding frequency region of the rotational transition of AlS ($^2\Sigma^+$). (a) N=6-5 (Cernicharo et al. 1988) toward Sgr B2, and (b) N=8-7 (Guélin et al. 1987b) toward IRC+10216.

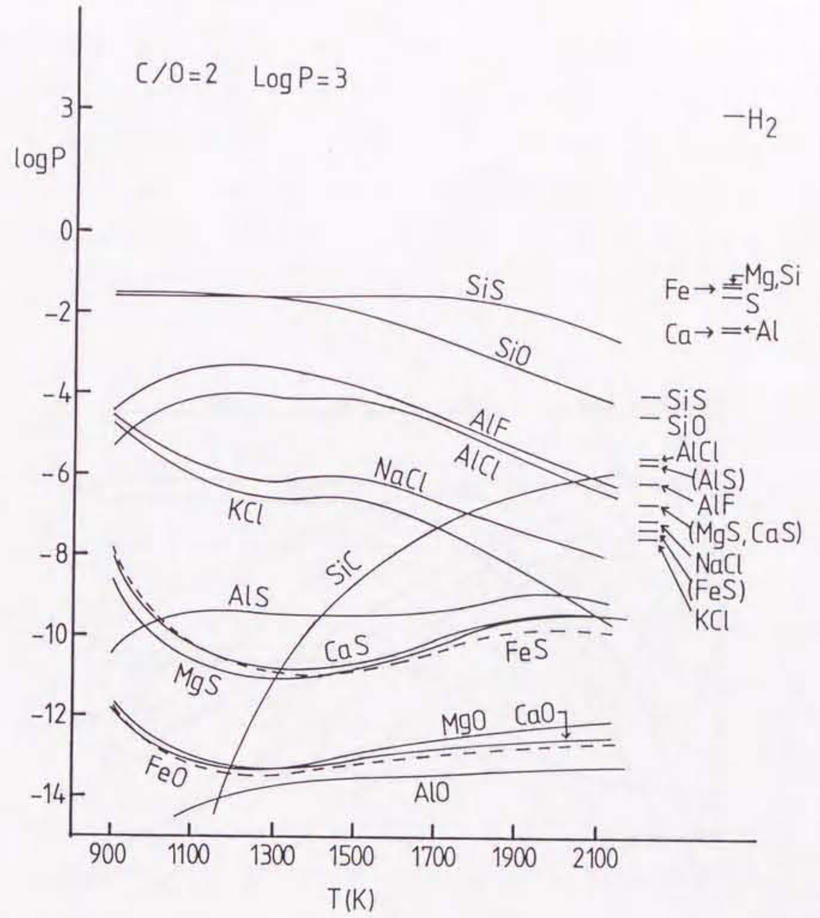

Figure 6: The calculated abundances of molecules for IRC+10216 by using thermal equilibrium calculation. The ordinate is the partial pressure of the molecules. The adopted total pressure is 10^3 dyn cm $^{-2}$, and the C/O ratio 2.0 (carbon-rich condition). At the right side of the Figure, the observed fractional abundances (including upper limits) for molecules, and the fractional cosmic abundances for atoms (relative to H_2) are shown.

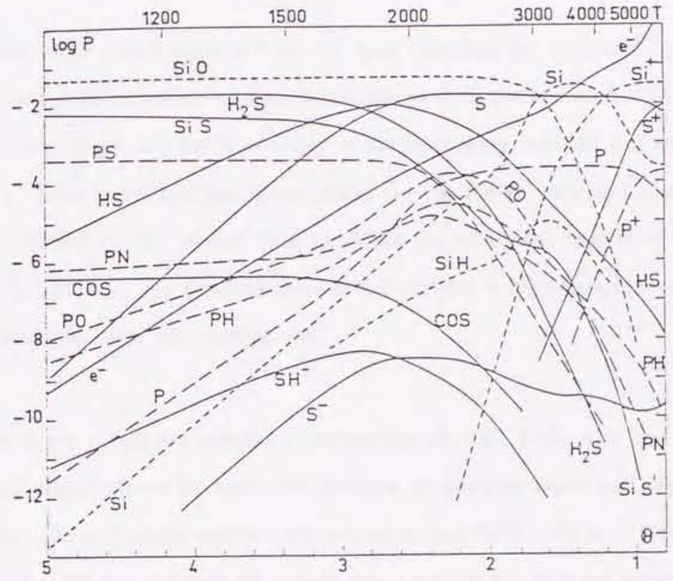

Figure 7: The calculated abundances of SiO, SiS and other molecules assuming thermal equilibrium in stellar atmospheres in oxygen-rich condition (Tsuji 1973). The ordinate is the partial pressure of the molecule.

Summary

(1) In the circumstellar envelope of late type stars, the molecular formation occurs. In particular, various molecules have been detected in the carbon-rich envelope of IRC+10216 by radiotelescopes, but Mg, Ca, and Fe containing molecules have not been detected in spite of the high cosmic abundances of Mg, Ca, and Fe. The behavior of these refractory elements is not well known, and is important to study the molecular processes and the dust formation mechanism. According to the thermal equilibrium calculation, metal sulfides (MgS, CaS, and FeS) are considered to be relatively abundant as carriers of Mg, Ca, and Fe.

(2) However, these metal sulfides have not been searched for in space, because the spectroscopic data of the accurate rotational transitions were not reported. The production of metal containing molecules is not easy in the laboratory, and the millimeter-wave spectroscopy of these metal containing molecules (in particular, radicals) is a new important field. Therefore, the author tried to obtain the rotational spectra of the metal sulfides in the laboratory. To produce these metal sulfides, a high-temperature absorption cell containing an oven was constructed.

(3) The accurate rotational transition frequencies of MgS, CaS, AlS, and FeS were obtained. MgS was produced by a reaction between magnesium vapor and sulfur vapor. CaS was produced by a reaction between calcium vapor and OCS. AlS is a $^2\Sigma$ radical and was produced by a reaction between aluminum vapor and OCS. FeS can be produced in a high-temperature cell, but it was more efficiently produced in a free space cell by stainless steel hollow cathode discharge in a mixture of Ar and H_2S. As a result, a complex electronic structure was revealed. The ground electronic state is considered to be $^5\Delta_i$. In addition, a low lying Σ state was found. Furthermore, as a new experimental method, the stainless steel hollow cathode discharge was found to supply iron to the gas phase. This

is a stable and convenient method, and this technique may be applicable to other metals.

(4) The four metal sulfides, MgS, CaS, AlS, and FeS were searched for mainly in the envelope of IRC+10216. However, the spectral lines were not detected, and the upper limits to the column density were determined. The upper limits were $2 \sim 3$ orders of magnitude smaller than the one of the abundant metal sulfides SiS. According to a thermal equilibrium calculation for the carbon-rich condition, the metal sulfides are definitely more abundant than the metal oxides. However, the calculated abundances of the metal sulfides are lower than their upper limit by $2 \sim 4$ orders of magnitude. This is because the abundance of SiO decreases as the C/O ratio increases in the carbon star, that is, the abundance of SiS increases, and as a result, most of the sulfur atoms are converted into SiS and the abundances of other metal sulfides decrease heavily. In addition, there is no efficient production mechanism for these metal sulfides except thermal equilibrium reaction, though such efficient production mechanisms are suggested for some molecules containing refractory elements; CP and SiC. Thus, the observational results obtained in this study is consistent with the thermal equilibrium model of the carbon-rich star.